Characterization Techniques for Photonic Materials

by

Bharati Neelamraju

A Thesis submitted to the faculty of

COLLEGE OF OPTICAL SCIENCES

In Partial Fulfillment of the Requirements

For the Degree of

MASTER OF SCIENCE

In the Graduate College

THE UNIVERSITY OF ARIZONA

2016

Statement by Author

The thesis titled *Characterization Techniques for Photonic Materials* prepared by *Bharati Neelamraju* has been submitted in partial fulfillment of requirements for a Master's Degree at the University of Arizona and in the University Library to be made available to borrowers under rules of the Library.

Brief quotations from this thesis are allowable without special permission, provided that an accurate acknowledgement of the source is made. Requests for permission for extended quotation from or reproduction of this manuscript in whole or in part may be granted by the head of the major department or the Dean of the Graduate College when in his or her judgement the proposed use of the material is in the interest of scholarship. In all other instances, however , the permission must be obtained from the author

SIGNED : Bharati Neelamraju

APPROVAL BY THESIS DIRECTOR

This thesis has been approved on the date shown below.

_____ May 2, 2016

Robert A. Norwood Date
Professor (College of Optical Sciences)

_____ May 2, 2016

Palash Gangopadhyay Date
Associate Research Scientist (College of Optical Sciences)

Acknowledgements

I would like to thank Prof. Robert A. Norwood for his continuous support and mentoring throughout my Masters Degree. I would like to give a special thank you to Dr.Palash Gangopadhyay, who always helped me with my research and guided me whenever required. I would also like to thank Dr. Gregory Cohoon for help with theLabView programming and making my experimental data acquisition system more robust. Another thank you goes to my family, specially my parents who have always supported me unconditionally in all aspects.

Contents

List of Tables

List of Figures

Abstract

The advancement of photonics technologies depends on synthesis of novel materials and processes for device fabrication. The characterization techniques of the optical, electrical and magnetic properties of the synthesized materials and devices, by non-contact, non-invasive and nondestructive methods plays a significant role in development of new photonics technologies. The research reported in this thesis focuses on two such aspects of photonic materials characterization : Magneto-Optic characterization and Spectroscopic Ellipsometry. The theoretical and experimental basis of these two techniques, and experimental data analysis are presented in two parts. In Part 1, the changes in magneto-optic parameters of FePT PS-P2VP block copolymer nanocomposites with increasing concentrations of FePt nanoparticles in the block copolymer are analyzed . We present the results of change in MO anisotropy factor with the wt% of FePt and try to analyze these changes with further experimentation. Part 2 presents the results of spectroscopic ellipsometry of group III-IV multilayered thin film materials to give their precise thicknesses and optical constants. Both these techniques are unique ways to understand novel material characteristics for future use in device development.

Introduction

Significant scientific and technological interest exists in both nanopolymer composites and structured thin films as they open new possibilities in tailoring material properties for electronic, photonic and magneto-optic device development for imaging, data storage and sensing and various other applications. Nanostructures are incorporated in most types of devices to increase efficiencies through better control and modulation of light-matter interactions at wavelength and sub-wavelength scales. Different semiconductor and polymer materials and nanostructures are being investigated for their potential applications in a wide range of photonic devices. Fabrication and manufacture of such devices requires precise control over the materials composition and morphology. A crucial step in achieving and verifying such control is the adoption of methods for non-destructive optical, electrical and magnetic characterization of materials and devices.

This thesis focuses on two important non-destructive approaches to the characterization of photonic materials and devices based on the interactions of light and matter; spectroscopic ellipsometry and magneto-optic methods. Spectroscopic ellipsometry helps determine the fundamental optical absorption, transmission and dielectric properties of materials. Magneto-optic (MO) characterization determines how these properties change in the presence of a magnetic field. In this thesis, both types of characterizations are addressed. Typically, the optical properties are important for design and fabrication of devices for electronic and energy applications, and the MO properties are central to device development for magnetic storage, sensing and biomedical applications. The MO properties are analyzed for FePt PS2VP nanopolymer block composites. Spectroscopic ellipsometry is used for the optical characterization of multilayer inorganic thin films of Group III-V semiconductors fabricated for application in various devices. Both types of materials were fabricated by collaborating groups at UA and elsewhere.

I. Spectroscopic ellipsometry

Spectroscopic ellipsometry helps to characterize the optical properties of thin films in terms of their thickness and fundamental absorption, transmission and dielectric properties. The knowledge of these properties in multilayer thin films is a prerequisite for comprehensive

optoelectronic device design, and is particularly important for sophisticated device architectures, such as tandem solar cells. The basic working principle of ellipsometry relies on measuring the change of the light beam polarization state after interacting with the thin film sample. This change is described by the two ellipsometric values Ψ and Δ, which represent the amplitude ratio and phase difference between *p*- and *s*-polarization. The detailed theoretical background is presented in subsequent chapters. This study focuses on spectroscopic ellipsometry of Group III-V semiconductor multilayer thin films to enable verification of the device structure and assessment of their potential application in optoelectronic devices.

II. Magneto-Optic Characterization

Magneto-optic characteristics of materials are determined based on the interaction of light and matter in the presence of a magnetic field. The MO properties arise from different effects of these interactions. Significant among these effects are the Faraday effect (also known as magnetic circular birefringence), magnetic linear birefringence (MLB), magnetic circular dichroism (MCD), Voigt effect, and magnetic linear dichroism (MLD). The presence of these effects depends on the frequency and polarization state of incident light, the direction of the magnetic field and how material absorption characteristics vary with the polarization state of the light. These effects and their theoretical basis are described briefly in the following chapters. This thesis focuses on the Faraday effect and depolarization in FePt block copolymer nano composites to provide basic data on the magneto-optic parameters. This can enable assessment of the potential of the nanostructured media for suitable applications.

Fundamental to both MO characterization and spectroscopic ellipsometry are the accompanying theoretical modelling of the magneto-optical and optical properties of the materials. Existing commercial modelling and simulation packages are used for modelling optical and magneto-optic properties. The research is of both fundamental and practical importance for current and future developments of material science and device development on the nanoscale.

III. Organization

This thesis is organized in two parts :

1. Part I: Spectroscopic ellipsometry of multilayer semiconductor thin films
2. Part II: Magneto-optic characterization of FePt nanopolymer composites

Each Part comprises four chapters, namely:

(i) Materials and properties, which introduces the materials analyzed and characteristics of interest

(ii) Experimental setup

(iii) Theoretical analysis, and

(iv) Results and discussion, which presents the detailed output from the experiments and analyses, and their implications

Part I : Spectroscopic Ellipsometry

1. Materials Analyzed

Spectroscopic ellipsometry is a powerful technique that can be use to acquire accurate knowledge of the refractive index, thickness and extinction coefficients of thin films[1].The knowledge of these effective optical constants is important for various applications [2].This part of the thesis contains a brief explanation of this technique and the tools needed for its data analysis. Four samples were analyzed - two samples each, with InP and polyacrylonitrile (PAN) substrates. The thickness of each layer of the four samples was analyzed using spectroscopic ellipsometry analysis (SEA) software. The ellipsometry data was taken using a SOPRA GES5E ellipsometer. In modeling the data, different methods were used in accordance with the material and the structure of the sample. The effective medium approximation was used in most cases to determine the optical constants of materials and account for surface roughness.

The two sets of materials analysed are,

- SiO_2 – Ag pair on PAN substrate
- InGaAs-AlInAs multi-layers on InP substrate

A dielectric host matrix (like SiO_2) embedded with nobel metal (like Ag or Au) nanoparticles are being studied by various groups due to their novel optical properties which can be used at a device level for various applications like photovoltaics.These properties of the nanoparticles are studied by Raman spectroscopy, optical transmissions/absorption, reflection, and spectroscopic ellipsometry. The physical characteristics of these metal nanoparticles influence the surface plasmon resonance.Hence the use of proper characterization techniques for understanding the behavior of these novel materials is important for research and development[3].

InGaAs and InAlAs are alloy semiconductors often used in electronic and opto-electronic heterostructured devices like distributed feedback lasers, quantum cascade lasers, etc. They are usually grown on an InP substrate because of their similar lattice structures[4]. The structural and electrical properties of these multi-layer heterostructures are dependent on growth parameters like temperature, pressure, rate of deposition etc. Therefore, the measurement of optical constants and thickness are important for device development.

2. Experimental Setup

2.1 Fundamentals

Ellipsometry is an optical non-invasive technique. It measures the layer thickness and optical functions of each layer in a multilayer structure. It is a highly sensitive approach, because it is based on measuring the phase shift of a light beam travelling through a layer structure. The measured parameters contain the physical properties of the layer structure, such as the layer thickness and refractive index but in a highly non-linear form. This technique measures the ratio of the complex Fresnel reflection coefficients. These ratios are defined by the ellipsometric angles, Ψ and Δ. These parameters contain the physical properties of the layer structure, such as the layer thickness and refractive index. As this is a transcendental and highly nonlinear equation, it needs to be solved by numerical methods, on a model-based approach. During this procedure, the layer structure is considered with thickness and optical functions in the model. The relative phase shift is calculated and compared to measured quantities during a numerical regression procedure[5]. Ellipsometry, in broad terms deals with phase and amplitude of the optical wave and the relationship between the *s* and *p*-polarized wave[6].

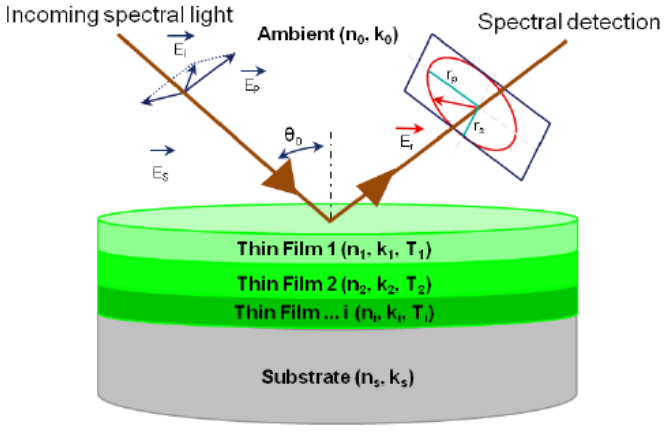

Figure 1: *Schematic of ellipsometry on a multi-layered thin film structure.*

The ellipsometry equation [6]:

$$\rho = \tan\Psi \; e^{i\Delta} \tag{1}$$

$$|\rho| = \tan\Psi = |R^p| / |R^s| \tag{2}$$

$$\Delta = \delta_1 - \delta_2 \tag{3}$$

Where :

- Ψ is an angle defined as above.
- Δ and Ψ are the measured quantities in the ellipsometer.
- δ_1=the phase difference between *p* and *s* planes before reflection
- δ_2=the phase difference between *p* and *s* planes after reflection
- Δ =induced phase shift due to reflection

2.2 The Ellipsometer

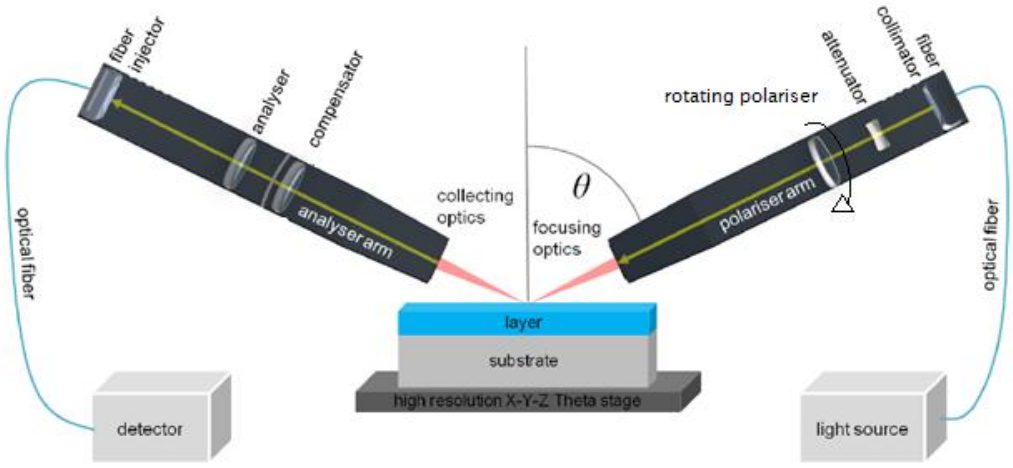

Figure 2 : *Schematic of the Sopra Spectroscopic Ellipsometer*

Basic Optical Components [6] :

Source : Sources can be lasers or arc lamps. Both these sources have their advantages and disadvantages. In our equipment we use an arc lamp which has a broad wavelength range (200-2000nm) but has focusing issues that can make it difficult to acquire noise free data.

1. **Polarizer/ Analyzer**: Convert the light beam of any polarization state to a light beam of single known polarization state (electric field component along the optical axis of the polarizer).
2. **Compensator (retarder/quarter wave plate)**: This component alters the phase of one polarization component of the light beam with respect to the other.
3. **Monochromator**: A monochromator is an optical device that transmits a mechanically selectable narrow band of wavelengths of light or other radiation chosen from a wider range of wavelengths available at the input.[7] The device used to separate light into its various spectral components could be a prism or a diffraction grating.
4. **Detectors**: There are 3 basic detectors that can be used for ellipsometric measurements - photomultiplier tubes (old technology), semiconductor photodiodes and CCD arrays.

1.3 Experimental Procedure :

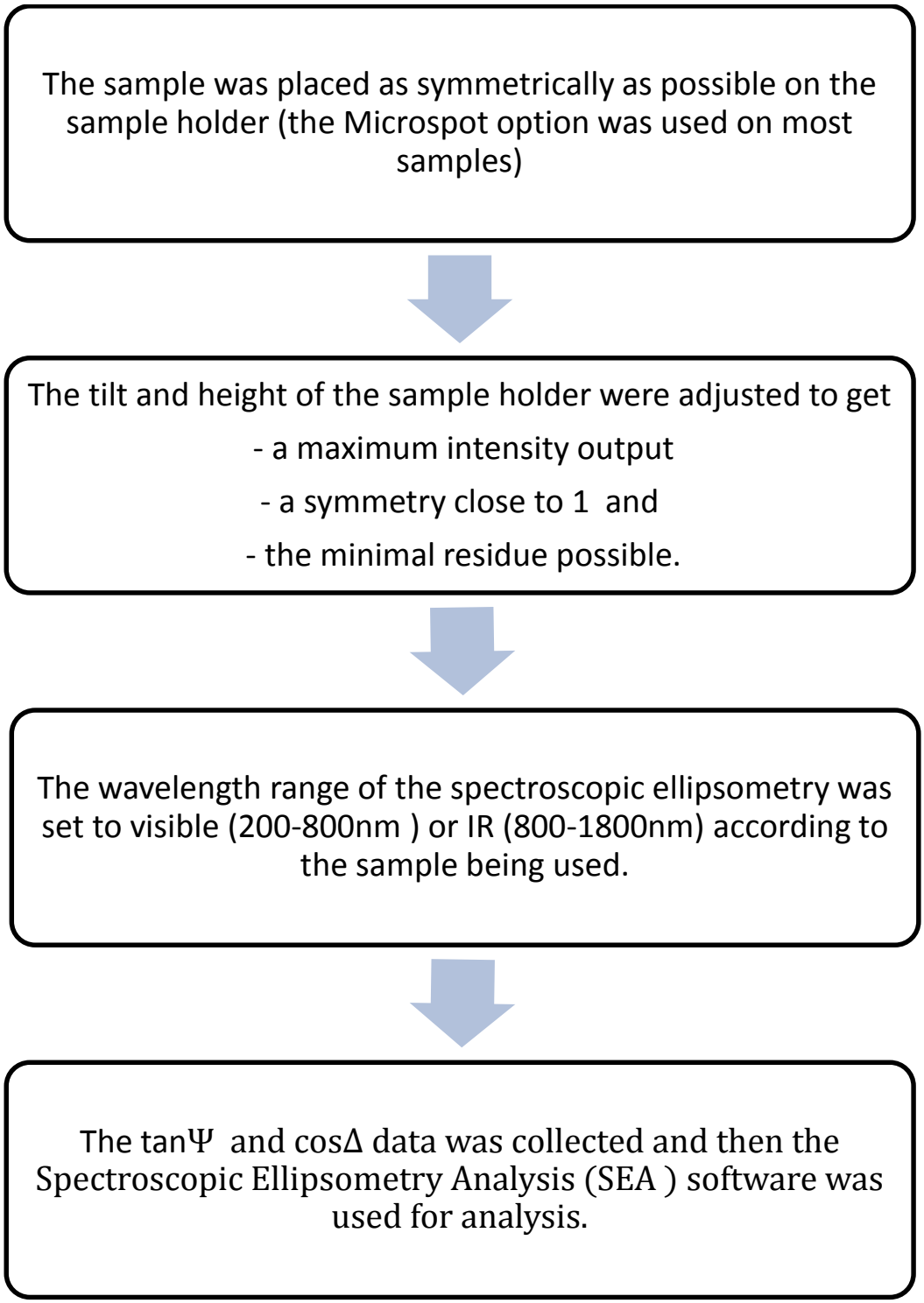

3. Theoretical Analysis

Data analysis proceeds as follows: An approximate model is constructed (using SEA software) to describe the sample's structure. The model is used to calculate the predicted response from Fresnel's equations (and the fundamental equation of ellipsometry equation) which describe each material with thickness and optical constants. If these values are not known, an estimate is taken for the purpose of initialization. The calculated values are compared to experimental data. Any unknown material properties can then be varied to improve the match between experiment and calculation. Usually the number of unknown properties should not exceed the amount of information contained in the experimental data. Finding the best match between the model and the experiment is typically achieved through regression. An estimator, like the R-squared value or the mean squared error (MSE), is used to quantify the difference between curves. The unknown parameters are allowed to vary until an R-squared value of close to 1 or a minimum MSE is reached.[8]

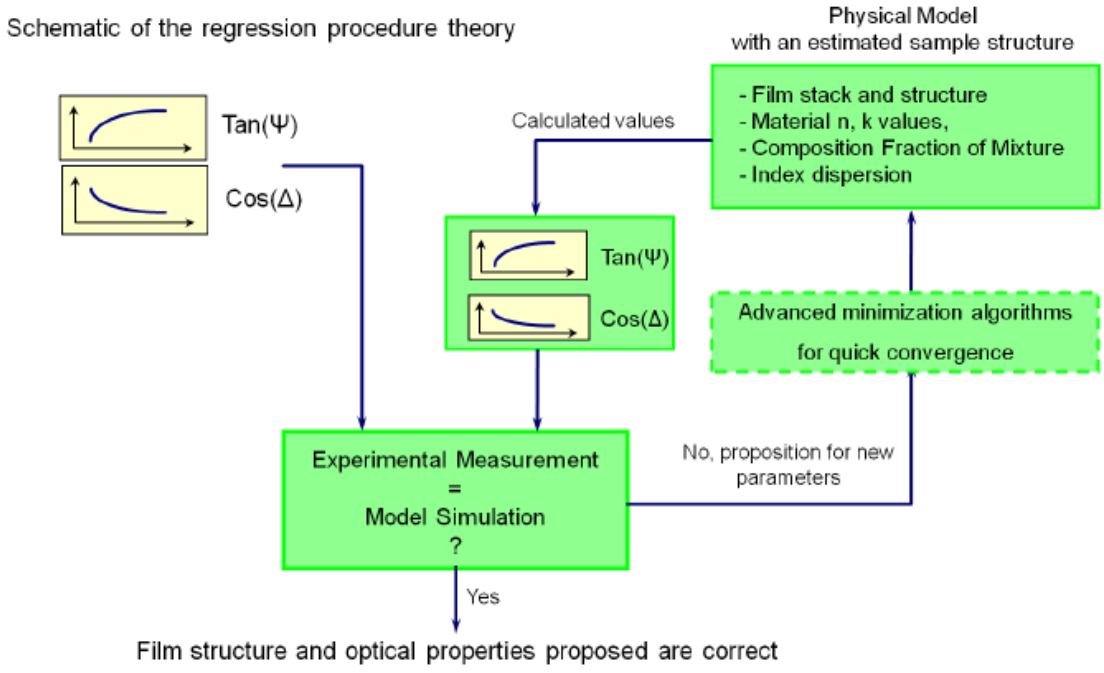

Figure 3: *Schematic of the regression procedure theory*

1.1 Important Observations

- When n is independent of wavelength:[6]
    1. maxima are further apart for longer wavelengths
    2. increasing thickness, causes movement of maxima/minima to higher wavelengths
    3. thicker films have more maxima/minima.
- When n depends on wavelength:
    1. at the maxima, the reflectance is identical to reflectance of film free substrate
    2. the upper envelop is the substrate alone
    3. effect of the thin films is to reduce this reflectance.
- Anatomy of the ellipsometric spectrum :

    Range of Δ and Ψ are defined as :

$$0 \leq \Delta \leq 180°;\ 0 \leq \Psi \leq 90°$$

    1. Spectra of the substrate :
        - any unknown surface film or roughness changes the *n-k* values
        - for any film free substrate

$$0 \leq \Delta \leq 180°\ ;\ 0 \leq \Psi \leq 45°$$

        - $\Psi > 45°$ implies the sample has atleast one thin film on the substrate.
    2. Spectra with a film :
        - spectral location of the Ψ minima depends on the thickness and optical constant of the film as well as the substrate
        - the value of this Ψ minima is dependent only on the substrate.
        - increase in thickness of the film brings the cusps closer together.
        - in a regression model :
            - thickness is increased to move the model to the right
            - thickness is decreased to move the model to the left.

1.2 Analytic Methods

A number of analytic methods are used for ellipsometric data fitting and analysis. Some of the methods used in our analysis are discussed below[8] :

1. Tabulated constants: The *n* and *k* data of some materials are in built in to the SEA software or can be obtained from literature and be used directly for data fitting.
2. Effective medium approximation (EMA): This approximation is usually used for composite materials. Maxwell-Garnett and the Lorentz-Lorenz model are used for heterogeneous mixtures. The Bruggeman model extends to include a larger range of materials.EMA with an ambient layer or void is used to compensate for surface roughness.
3. Dispersion relations: This is a more complex method of evaluation where we use a dispersion relation to describe the optical constants of a material. There are different models used depending on the material being used. Some examplesinclude:
    - Lorentz oscillator model for insulators, semiconductors and conductors
    - Cauchy model for semiconductors and insulators
    - Drude model for metals.
4. Regression analysis:A model of the structure is built with seed values for the thickness and optical constants for each layer. The regression analysis is then used to get the final thickness and optical constants by fitting the measured and calculated values.

4. Results And Discussion :

The results of ellipsometry analyses of the 4 different samples studied are presented.

4.1 In_72 final structure

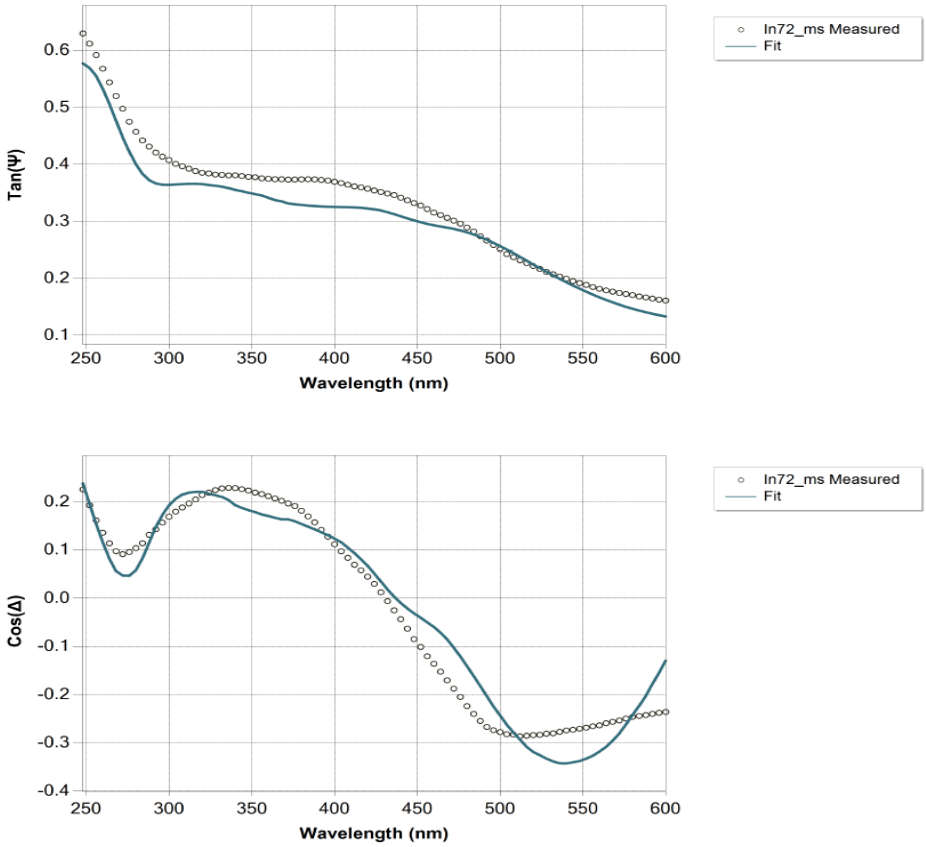

Figure 4 : *InP sample (In_72) ellipsometry data fitting*

Following are the details of the structure for the sample In_72 :

Phase	**Material**	**Approx. thickness (nm)**	**Analysed thickness by ellipsometry (nm)**	**Derived parameter - *n* (@ 632.8nm)**	**Derived parameter - *k* (@632.8nm)**
Phase 4	InGaAs	~2.5	13.5 (EMA)	3.2205	0.2639

Phase 3	AlInAs	~2.9	3.4	3.6296	1.3684
Phase 2	InGaAs	~9.6	22.6	3.9896	0.3792
Phase 1	AlInAs	~1700	1700	3.6296	1.3684
Substrate	InP	Infinity	Infinity	3.5354	0.3069

R squared value of 0.934 and RMSE of 0.0388 was achieved by using the structure mentioned above. *n-k*files were used for each Phase 1-3 and the EMA of InGaAs and void was used in Phase 4 to account for surface roughness.

4.2 In_73 Final Structure

The analysis of In_73 was similar to that of In_72

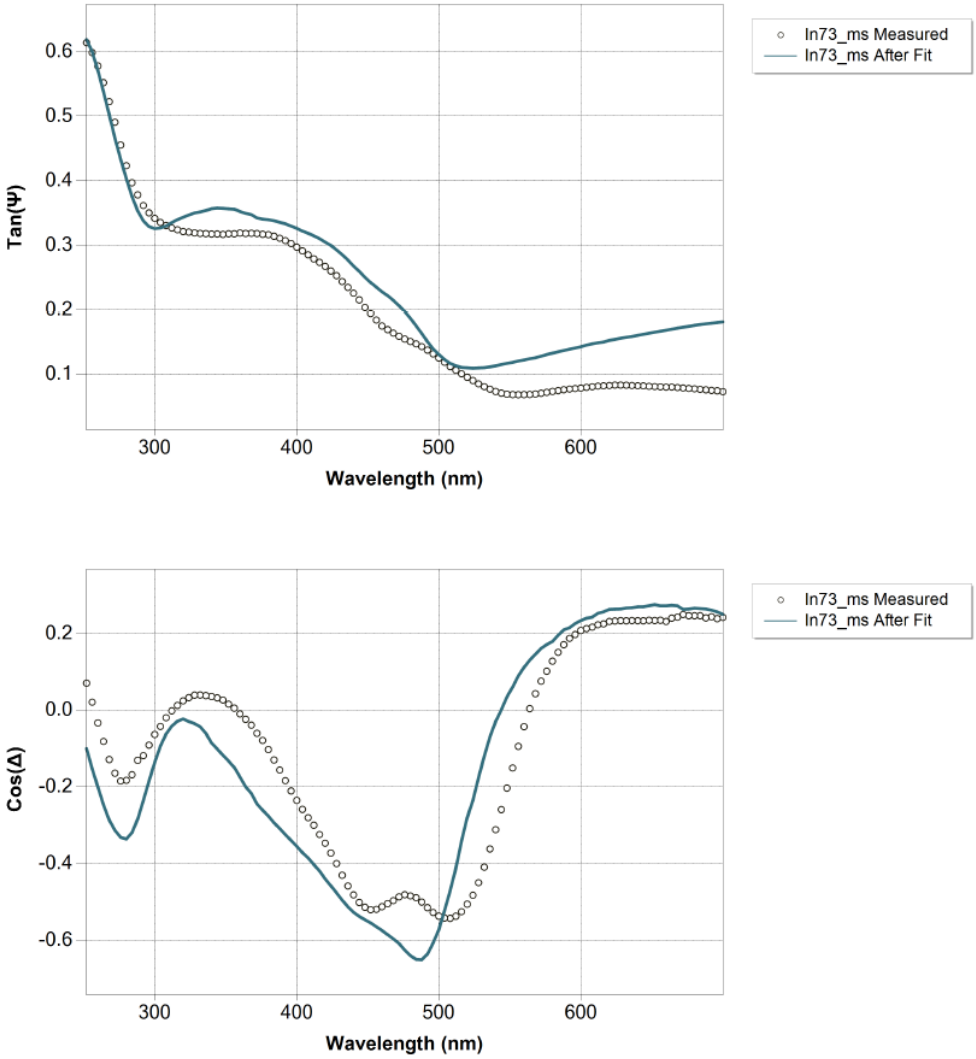

Figure 5 *: InP substrate (In_73) ellipsometry data fitting*

Phase	**Material**	**Approx. thickness (nm)**	**Analysed thickness by ellipsometry (nm)**	**Derived parameter - *n* (@632.8nm)**	**Derived parameter - *k* (@632.8nm)**
Phase 4	InGaAs	~2.5	10.8(EMA)	3.8315	0.3572
Phase 3	AlInAs	~202	156.1	3.6296	1.3684
Phase 2	InGaAs	~8.6	21.8	3.9896	0.3792
Phase 1	AlInAs	~1000	1330.9	3.6296	1.3684

Substrate	InP	Infinity	Infinity	3.5354	0.3069

R-squared value of 0.8282 and RMSE of 0.0952 was achieved by using the structure mentioned above.*n-k* files were used for each Phase 1-3 and effective medium approximation (EMA) of InGaAs and void was used in Phase 4 to account for surface roughness.

4.3 Ag_SiO_planar

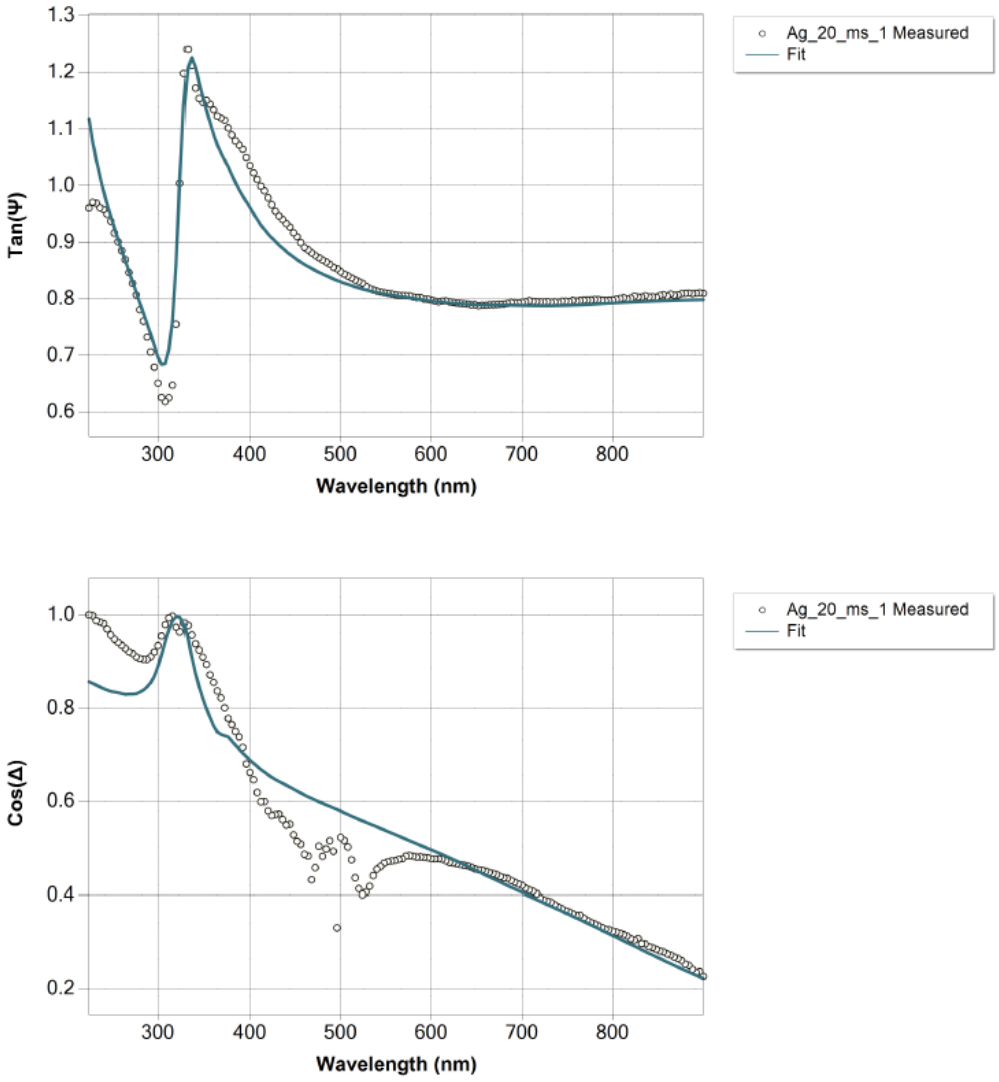

Figure 6 : *PAN substrate (sample 1) ellipsometry data fitting*

Phase	**Material**	**Analysed thickness by ellipsometry (nm)**	**Derived parameter - *n* (@632.8nm)**	**Derived parameter - *k* (@632.8nm)**
Phase 2	SiO_x (EMA)	24.9	1.4526	0
Phase 1	Ag	15.9	0.1352	3.9866
Substrate	PAN	Infinity	1.5105	0.0005

R-squared value of 0.9143 and RMSE of 0.05365 was achieved by using the structure mentioned above. *n-k*files were used for each Phase 1 and substrate while the EMA of SiO_2 and void was used in Phase 2 to account for surface roughness[2].

4.4 SiO_Ag_Planar

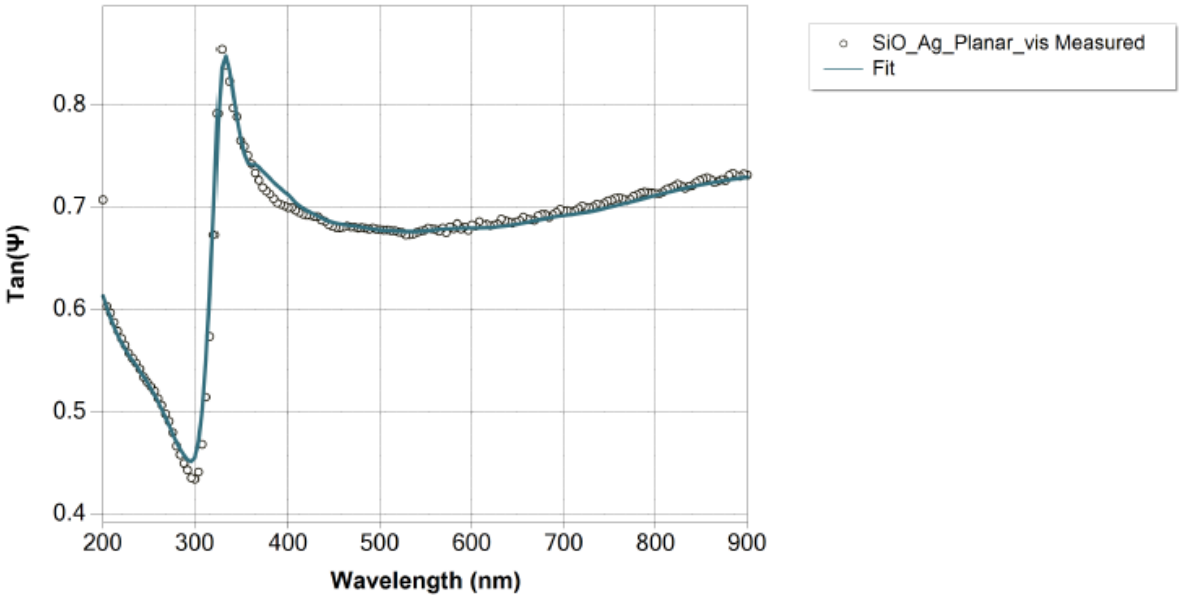

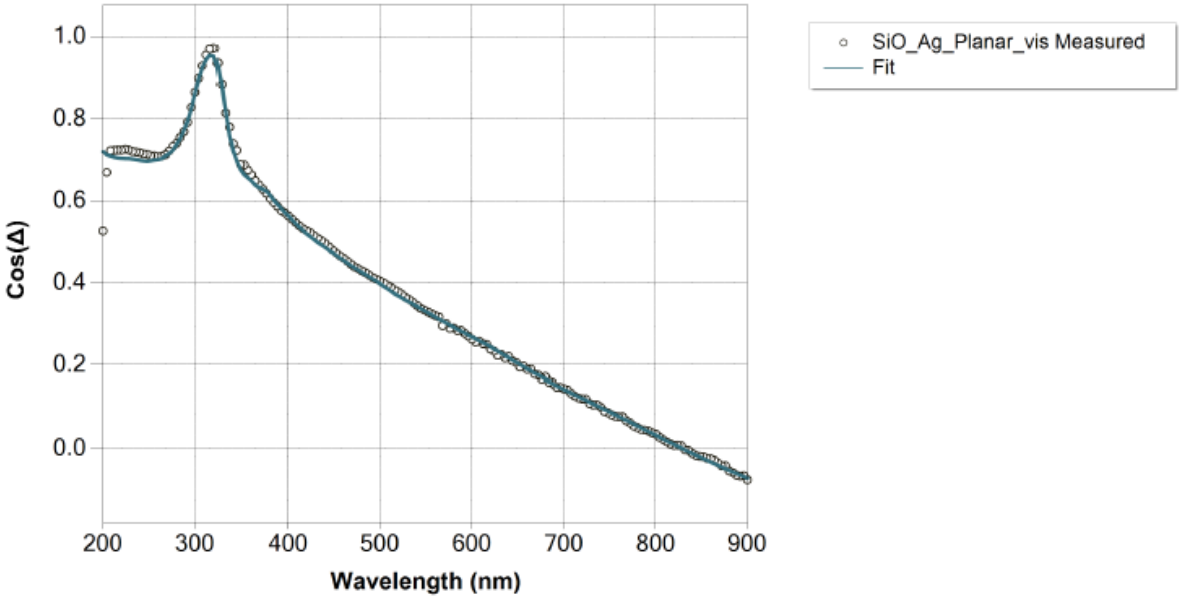

Figure 7*: PAN substrate (sample 2) ellipsometry data fitting*

Phase	**Material**	**Analysed thickness by ellipsometry (nm)**	**Derived parameter - *n* (@632.8nm)**	**Derived parameter - *k* (@632.8nm)**
Phase 2	Ag (EMA)	16.5	0.1337	3.9107
Phase 1	SiO2	4.6	1.457	0
Substrate	PAN	Infinity	1.5105	0.0005

R-squared value of 0.989 and RMSE of 0.0142 was achieved by using the structure mentioned above. NK files were used for each Phase 1 and substrate while the EMA of SiO_2 and void was used in Phase 2 to account for surface roughness[2].

4.5 Conclusion

- Thicknesses of both the InP samples were reported. Direct *n-k* files were used to model each phase and EMA was used to account for surface roughness.
- A PAN_Ag_SiO sample was analyzed and the thicknesses measured.
- PAN_SiO_Ag planar sample was analyzed. It was equivalent to a layer of Ag. This could be because PAN and SiO_x have similar refractive indices.

Part II :Magneto-Optic characterization

1 Magneto-optic Characterization : Materials and Properties

The recent increase in demand for low cost integrated photonics components in the optical communications industry has led to extensive research on novel technologies for high yield manufacturing processes. Polymer based technologies are low-cost and getting more efficient by the day. However, targeted polymer based magneto-optic applications such as integrated optical isolators are yet to be commercialized. Research in this area is hence important for the growth of technology.

Materials with possibly high MO Verdet constant are required for development of both free-space and integrable magneto-optic devices. The Verdet constant is an important magneto-optic characteristic of materials that provides a quantitative measure of its faraday rotation ability. The Faraday effect or faraday rotation refers to the rotation of the polarization plane of a polarized light beam incident on an optically thin material kept in a magnetic field parallel to the direction of propogation of light. The faraday rotation is directly proportional to the strength of the magnetic field and the length of the sample, the Verdet constant representing the constant of the proportionality. (The theoretical background of the faraday rotation is presented in later sections)

Faraday rotation is a useful property because it lets us determine magnetic properties by optical measurements which are non-invasive. Due to high absorption in bulk materials, Faraday rotation is usually measured only in relatively thin films. While large Faraday rotations have been observed in transparent compounds such as terbium gallium garnett (TGG), they work only in a single crystal geometry to minimize light scattering. Hence an easier method of production of MO active materials is a goal of a number of research groups. Nanocomposites with ferromagnetic nanoparticles dispersed in polymer and glass matrices is one such alternative for processable MO materials with high activity.[1]

1.1 Material overview – FePt block copolymer nanocomposites

Polymer-nanoparticle composites, where the polymer is the prime transparent passive host for various metal, metal oxide and semiconducting nanoparticles have emerged as major sources

of new materials for devices owing to their unusual optical, electronic, and magnetic properties. In the particular case of self-assembled block co polymers, it has been shown that they can provide a low-cost and more flexible process for design, fabrication and manufacture of photonic devices over more complex approaches like lithography[2]. Further, magnetic nanoparticles (NPs) have been shown to have a wide range of applications in microelectronics such as spin-dependent electron transport, high-density magnetic storage, magnetic isolators, low field sensors, etc., and biomedicine[3]. The main challenge for MO devices with magnetic NPs is to push the superparamagnetic limit towards smaller particle sizes. (In the superparamagnetic state, a nanoparticle possesses a large magnetic moment and fast response to applied magnetic fields with negligible remanence and coercivity. Superparamagnetism of magnetic nanoparticles is the fundamental density limit for magnetic memory devices and in biomedical applications such as MRI). This requires production of nanopolymer composites in which the nanomagnets have minimum dimensions with spatially and temporally stable magnetization [4]. However, the magnetization value of a superparamagnetic nanoparticles depends not only on the size, but also on their magneto-crystalline anisotropy. Hence, the search for the right magneto-optic material and their proper characterization is an important problem for research in magneto-optics.

FePt block copolymer nanocomposites have emerged as one such set of nanocomposite materials which fit these requirements. FePt nanoparticles are thermally stable and ferromagnetic even at as small diameters as 3 nm. When self assembled in a tightly packed array and with control of magnetic axis direction, they can be ideal candidates for magnetic storage media [3].

FePt block co-polymer nanocomposites which are self assembled magnetic NP structures in PMMA polymer on a glass substrate are used in this study. They contain equal atomic percentage of Fe and Pt. The crystal structure of FePt is a chemically ordered face-centered tetragonal (fct) structure which is chemically more stable than high moment nanoparticles such as Co and Fe.

Most of the research on FePt nanoparticles to date has mainly focused on synthesis methods for producing FePt nanoparticles with controllable particle size and a narrow size distribution which can be transferred into the ordered phase readily by annealing. Further research is required

to obtain a more fundamental understanding of the magnetic properties of FePt nanoparticles as the magnetic properties have been shown to depend strongly on particle composition, size and crystal structure.

1.2 Properties of materials

This section defines and elaborates on the properties studied during the course of the thesis. The magneto-optic properties are discussed in detail, while some important material characteristics are also defined.

1.2.1 General Properties

Some properties of significance include [5]:

- **Anisotropy,** the tendency of a material to have properties that are directionally dependent.
- **Birefringence,** the retardance associated with propagation through an anisotropic medium. For each propagation direction within a birefringent medium,there are two modes of propagation with different refractive indices.
- **Retardance (*α*), the** polarization-dependent phase change associated with a polarization element or system. The phase (related to the optical path length) of the output beam depends uponthe polarization state of the input beam. The transmitted phase is a maximum for one eigenpolarization, and a minimum for the other eigenpolarization.
- **Depolarization (β), the** process which couples polarized light into unpolarized light. It is intrinsically associated with scattering, diattenuation andretardance which vary in space , time, and/or wavelength.
- **Diattenuation,** the property of an optical element or system whereby the intensity/transmittance of the exiting beam depends on the polarization state of the incident beam .
- **Dichroism**, the material property of displaying diattenuation during propagation . Foreach direction of propagation, dichroic media have two modes of propagation with different absorption coefficients. Examples of dichroic materials include sheet polarizers and dichroic crystals such as tourmaline .

1.2.2 Magneto-optic properties

A **magneto-optic effect** can be any phenomena in which an electromagnetic wave propagates through a medium that has been altered by the presence of a quasistatic magnetic field [6]. (A quasistatic process is one that happens slowly enough for the system to remain in internal equilibrium). MO effects can be best described in terms of the dielectric tensor (ε) of the medium where the incident light beam interacts with the applied magnetic field.

$$\varepsilon = \begin{bmatrix} \varepsilon_{xx} & \varepsilon_{xy} & \varepsilon_{xz} \\ \varepsilon_{yx} & \varepsilon_{yy} & \varepsilon_{yz} \\ \varepsilon_{zx} & \varepsilon_{zy} & \varepsilon_{zz} \end{bmatrix} \tag{4}$$

Now, a static magnetic field is applied to an isotropic medium in the direction of propagation of light (z). The dielectric tensor ε of the MO material then governs the light-matter interactions.

$$\varepsilon = \begin{bmatrix} \varepsilon & -i\varepsilon_{xy} & 0 \\ i\varepsilon_{xy} & \varepsilon & 0 \\ 0 & 0 & \varepsilon \end{bmatrix} \tag{5}$$

Fig(8) below explains graphically the effect of magneto-optically active media. The green arrow in the figure is the electric field vector (polarization direction) Fig (8b) shows the vanishing of the off-diagonal elements i.e. when there is no MO effect. Fig (8c) shows the rotation of plane of polarization due to real ε_{xy} and Fig (8d) shows the rotation of plane of polarization because of the imaginary ε_{xy} where the output polarization is elliptical due to absorption effects[7].

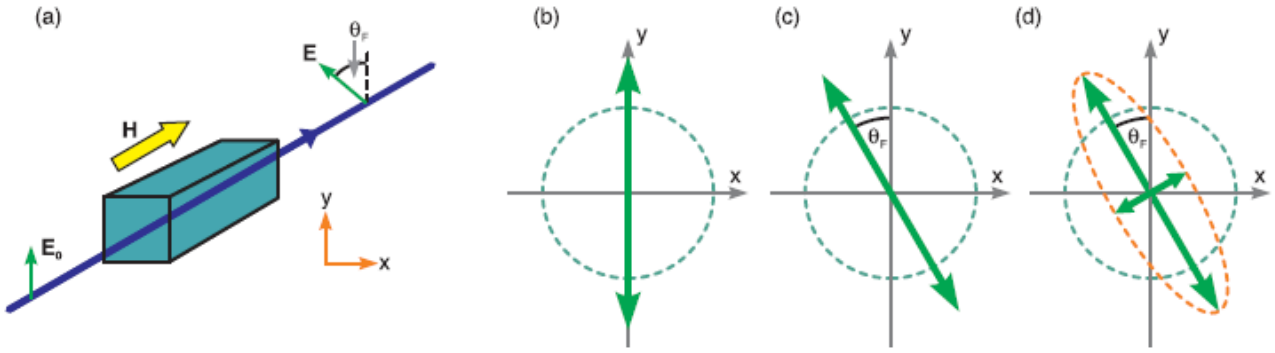

Figure 8 : *Propagation of a linearly polarized beam through a longitudinally magnetized medium in three different scenarios [10]*

Now the ability of a particular material to rotate the electric field vector is quantified by the Verdet constant (V_B) of the materials

$$V_B = \frac{\theta_F}{BL} = \frac{\varepsilon_{xy}\pi}{\lambda n B} \tag{6}$$

where θ_F is the Faraday rotation, B is the applied magnetic flux density and λ is wavelength of input EM wave (laser).

MO effects can be broadly categorized into two : Transmission and Reflection (Fig9) effects [6] . Reflection effects have three geometries : the polar Kerr effect, longitudinal or meridonal Kerr effect and equatorial Kerr effect as shown in the Fig 9.

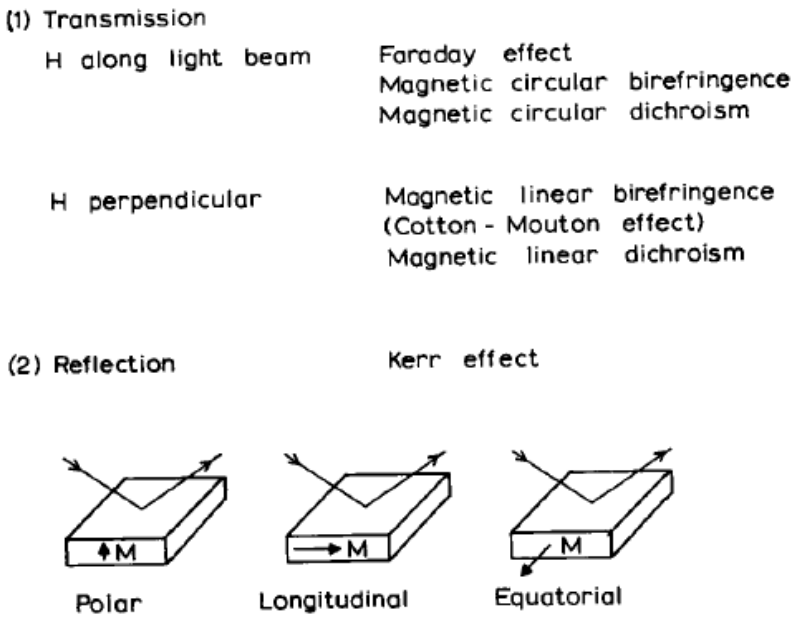

Figure 9: *Summary of principle magneto – optic effects*

The transmission effects have two geometries: the Faraday geometry which is longitudinal and $\mathbf{k}\|\mathbf{H}$, or the Voigt geometry which is transversal and $\mathbf{k}\perp\mathbf{H}$. All the MO effects addressed within this thesis are transmission with **H** parallel to the wave propagation **k,** i.e., the Faraday geometry. The effects include the following:

- magnetic circular birefringence
- magnetic circular dichroism, and
- Faraday effect

The presence of these effects depends on the input polarization state of light, the magnetic field and absorption of the material. These effects are described briefly to differentiate their origin and fundamental characteristics:

1.2.2.1 Magnetic circular birefringence

"Birefringence" means double refraction. It applies to materials whose refractive index depends on the direction that light travels and its polarization. If the refractive index is different

for left and right circularly polarized light, this effect is called circular birefringence. The superposition of left circularly polarized (LCP) and right circularly polarized (RCP) light waves gives rise to linearly polarized light. Hence, a circularly birefringent medium will slow down the two circular polarizations of light (RCP and LCP) to different extents. Materials that rotate the plane of polarization of the light travelling through them (regardless of input polarization and propagation direction) are called optically active materials. Hence, optical activity is caused by circular birefringence or circular dichroism. Essentially, "circular birefringence rotates the plane of polarization of incident linearly polarized light."[8]

Now, magnetic linear birefringence is an optical activity that arises in the presence of a magnetic field. Magnetic circular birefringence (MCB) on the other hand is defined as "**the field-induced difference in refraction of the left and right circularly polarized components of light that is incident parallel to the magnetic field"**[9]. MCB is a universal effect and does not require any of the prerequisites for natural circular birefringence. MCB, like the natural circular birefringence also leads to the rotation of the plane of polarization of the linearly polarized light and is therefore also called magnetic optical rotation. This magnetic effect was discovered by Faraday in 1849 and is also called the faraday rotation. This particular discovery played an important role in establishing light as an electro-magnetic phenomenon and lead to various subsequent developments in science.[9]

1.2.2.2 Magnetic circular dichroism

"Dichroism" means that a material absorbs two different types of light differently. If the adjective "circular" does not precede it then it refers to linearly polarized light: simple dichroism is when a material absorbs light polarized in some plane differently than light polarized in a plane perpendicular to it. Materials having high dichroism can be used as *polar filters* because they are practically transparent to light polarized in one direction but practically opaque to light polarized in the perpendicular direction. Some materials absorb LCP light to a different extent that RCP light. This is called circular dichroism. Circular dichroism makes plane-polarized light elliptically polarized.

Magnetic linear dichroism is also an optical activity that arises upon placing matter in a magnetic field. Magnetic circular dichroism (MCD) is defined **as the field-induced difference in the absorption (or emission) of the left and right circularly polarized components of light that is incident parallel to the magnetic field**. MCD is also a universal effect and does not require any of the prerequisites for natural circular dichroism to occur. [9]

1.2.2.3 Faraday rotation

The rotation of the plane of polarization of incident linearly polarized EM wave due to the magnetic field induced circular birefringence of the material is called Faraday rotation. Hence, Faraday rotation is a consequence of magnetic circular birefringence. Faraday ellipticity on the other hand is a consequence of magnetic circular dichroism. In the figure (3) below, (a) in going through a slab of magnetic material, a linearly-polarized beam of light with its E-field along the X-axis acquires a component of polarization along Y. The lines of B-field shown within the medium represent either an externally-applied magnetic field or the intrinsic magnetization of the medium (b).

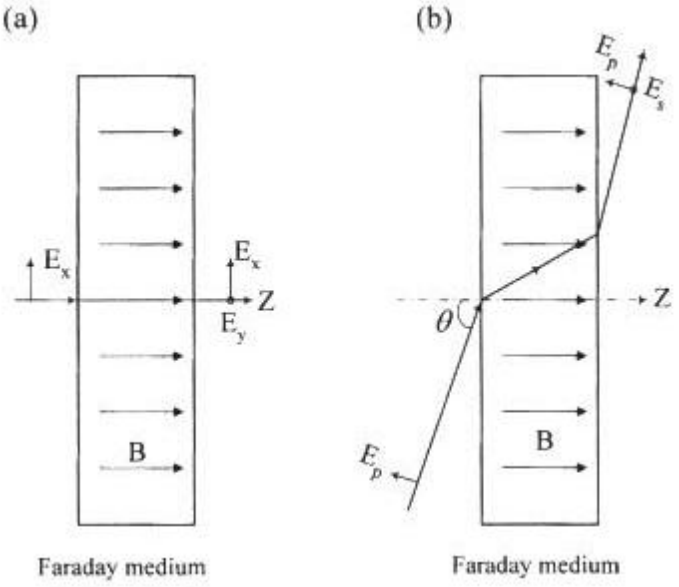

Figure 10 : *Pictorial depiction of the Faraday rotation*

The effect is also observed at oblique incidence. Shown here is a *p*-polarized incident beam, which acquires an*s*-component upon transmission through the magnetic medium. (If the incident beam were *s*-polarized, the magneto-optically induced polarization would have been in the *p*-direction.). The magneto-optically induced components of polarization change sign on reversing the magnetic field *B*[10]

However, the wavelength-dependence of the direction of the output polarization produces a certain amount of depolarization β in the emergent beam. The Faraday rotation combined with

the spectral bandwidth of the light source thus causes partial depolarization as a direct consequence of interference among the multiple reflection.[10]Hence, characterizing this depolarisation factor is also of importance. The Mueller matrix polarimetry approach (as shown in later chapters) works not only with cross-polarization effects, but can also describe the depolarization effects caused by surface roughness, line edge roughness or line width roughness[11].

The Faraday Effect is a complex quantity where the real part is the Faraday rotation θ_{FR} and the imaginary part is the Faraday ellipticity θ_{FE}

$$\Theta_{CFE} = \theta_{FR} + i\theta_{FE} \tag{7}$$

Now, experimentally these terms can be determined by measuring the second and third harmonics of the signal (lock-in amplifiers are used for these measurements).

$$\mathrm{Re}[\theta_{FR}] = \frac{1}{8J_2(\delta)}\frac{I_{2f}}{I_0} \text{ 2nd harmonic, 2f} \tag{8}$$

$$\mathrm{Im}[\theta_{FE}] = \frac{1}{8J_3(\delta)}\frac{I_{3f}}{I_0} \text{ 3rd harmonic, 3f} \tag{9}$$

$$Circ\Delta n \propto \mathrm{I}_{1f} \text{ 1st harmonic, 1f} \tag{10}$$

where ,

I_{2f} is the intensity of the second harmonic,

I_{3f} is the intensity of the third harmonic,

I_0 is the input intensity and

$J_n(x)$ is the Bessel function of order n

$\delta(t) = R_d \cos(f_{PEM}t)$,

In a composite material comprising a polymer matrix with dispersed nanoparticles, the scattering of light propagating in the composite decreases the optical transparency as the volume percentage or size of the nano particles or both increase. However, the Faraday Rotation (FR) increases with increasing nanoparticle size and concentration. Thus, the goal in MO materials design for optoelectronic applications is to achieve the optimal tradeoff between FR and optical

transparency of the bulk composites with respect to size and concentration of the particles in the host matrix. This thesis deals principally with the effect of the FePt nanoparticle concentration on the MO properties of the corresponding composites.

2. The Experimental Setup

The experimental setup designed for the Faraday rotation studies of FePt PS2VP nanopolymer composites (Fig 11) compromises multiple optical and other components : laser diode (source), half wave plate, quarter waveplate, non polarizing beam splitter, magnetic enclosure with sample holder, mirror, beam splitter, photo detectors, Wollaston prism, photoelastic modulator (PEM), auto-differential detector and lock-in amplifier. The details of the working of each component in the system are elaborated upon in this section of the thesis.

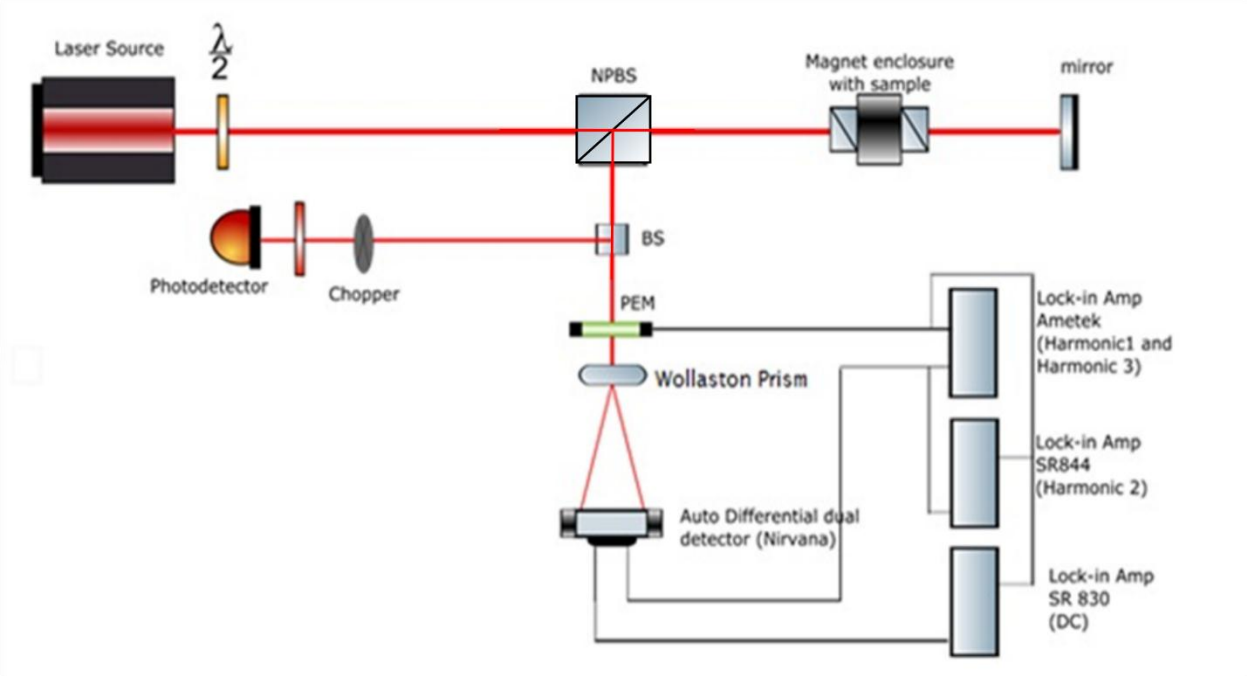

Figure 11: *Magneto-optic characterization setup*

The components in this setup were aligned using a 1310 nm IR diode laser for magneto-optic characterization of the FePT PSP2VP samples.

There are two ways linearly polarized light can change after interacting with a sample in a magnetic field:

2. the plane of the polarization can rotate and
3. the light can acquire ellipticity.

These polarization changes in the transmitted light are characterized by the complex Faraday angle (due to absorption).

The diode and semiconductor laser operating at different wavelengths were setup as described in figure (11) ; the diode lasers are at 980nm and 1310nm. All optics used are uncoatedand any retarder used to balance polarizations in the detectorswas wavelength specific.

A linear polarizer (analyzer) placed after the NPBS is oriented at 45° with respect to the *x* axis to mix the *x* and *y* polarization components of the light exiting the PEM. The intensity measured using a conventional photodetector is used to determine DC, 2f and 3f harmonics. The other half is split into horizontal and vertical polarization components by passing it through a Wollaston prism and a phase sensitive auto differential detector is used to detect the sign of the phase change and measure 1f and 2f signals. Note that here the harmonics are based on the PEM modulation frequency (f = 50kHz) and not the optical excitation frequency. Another lock-in amplifier is referenced to the chopper frequency (between 200Hz ~ 1 kHz) in order to measure the overall light intensity.[7]. The sensitivity analysis of this system is out of the scope of this thesis but can be a prospective research opportunity in optical instrumentation. This system's ability to measure microdegree Faraday rotation values however depends on the source wavelength, optical power, measurement time, bandwidth etc.[8]

By careful calibration and alignment of polarizers one can measure absolute amplitude and the direction of polarization changes using this setup. The Mueller matrix approach allows for calculation of optical and Faraday rotation, or Faraday ellipticity using the expressions listed in the subsequent chapters.

2.1 Setup Components

Some important components of this setup are described below :

2.1.1 Magnet Enclosure :

The Montana Instruments Magneto-optic module was used to provide the magnetic field. This particular module can go upto a 1Tesla magnetic field (theoretically) with very convenient

optical access and experiment flexibility. Optical access through the poles, high NA access from the sides, and low working distance access from the top make this instrument simple to setup. The magnet poles have a bore through the core to allow laser illumination of the sample. This preserves optical access from all four sides, as well as the top. The field strength depends on the configuration being used[1]. Figure (12)gives a pictorial representation of this enclosure in use in our lab.

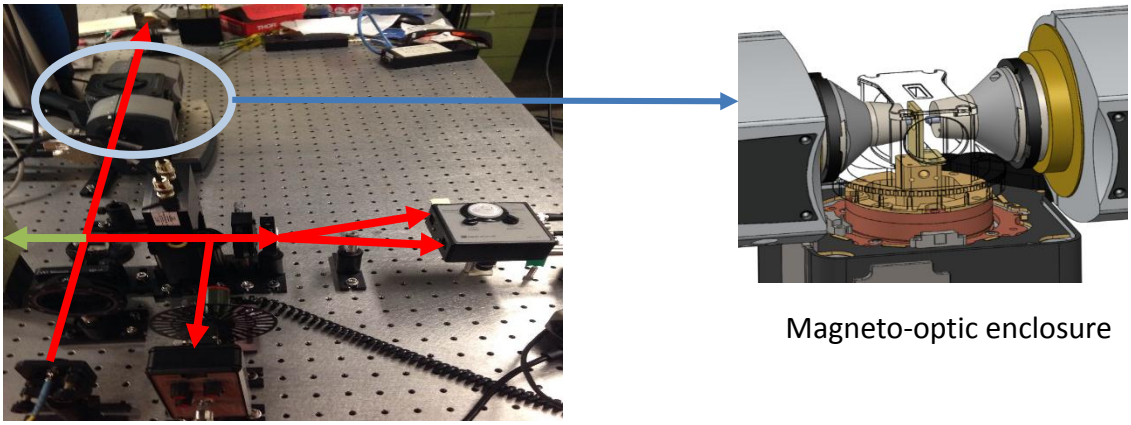

Figure 12: *Setup with the magnetic enclosure*

2.1.2 Photo-Elastic Modulator (PEM)

The photoelastic modulator (Fig 13) works on the principle of photoelasticity, in which a mechanically stressed sample exhibits birefringence proportional to the resulting strain. PEMs are resonant devices which produce an oscillating birefringence at a fixed frequency. It consists of a suitable transparent material (depending on wavelength in use) attached to a piezo-electric transducer which is tuned and driven by an electronic circuit that controls the amplitude of vibration.[2]

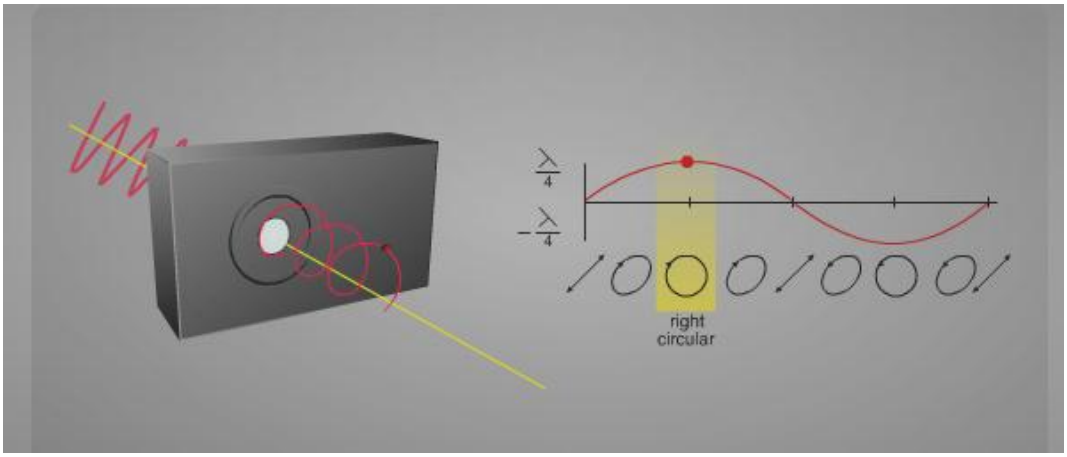

Figure 13: *PEM operating principle*

The PEM is usually used in either of two basic modes: as a modulator, to produce polarization modulation of a light beam, or as an analyzer, to determine the polarization state of a light beam.

Hind Instruments photoelastic modulator (PEM) with a fused silica active element was used for all measurements for lasers operating between 470nm to 1310nm. The photoelastic modulator (PEM) modulates the phase of the two orthogonal linear polarization components that pass through it. It is this modulation that allows us to determine the polarization of the beam that passes through the sample. The optical axis of the PEM is oriented along the *x*axis, which is the same orientation as the incident light polarization shown in the figure 13 above. After passing through the sample twice, the transmitted light acquires a small *y*-component of polarization, which produces rotation and ellipticity. The PEM modulates the phase of this *y*-component of polarization with respect to the *x*-component at a frequency $f_{PEM} \approx 50 \times (2\pi)$ kHz. The PEM modulates the phase difference between the *x* and *y* components of the transmitted light sinusoidally: $\delta(t) = R_d \times \cos(f_{PEM} t)$, where R_d is the dynamic retardance and is the phase modulation amplitude of the PEM.

2.1.3 Wollaston Prism

The Wollaston prism is a polarizing beam splitter that preserves the ordinary (*o*) and extraordinary (*e*) rays. It is made of two right triangle prisms with perpendicular optic axes. The beam diverges from the prism giving two perpendicularly polarized rays (S and P).[3]

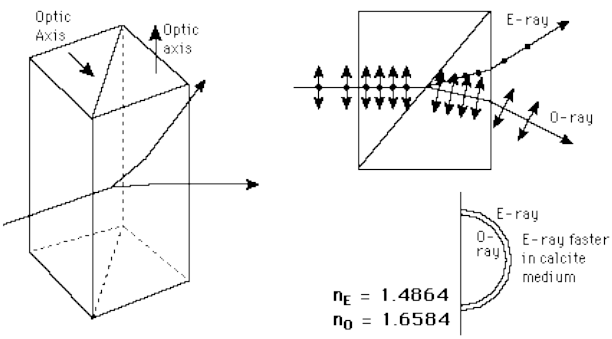

Figure 14: *Working of a Wollaston prism*

2.1.4 Autobalance Differential Dual Detector (Nirvana)

Nirvana detector is designed for use in a dual-beam setup: one invariant reference path and one signal path. This particular detector reduces common mode noise by over 50 dB at frequencies from DC to 125 kHz. Thus, we can effectively eliminate laser-intensity noise and make shot-noise limited measurements at low frequencies. It reduces noise by subtracting the reference and signal photocurrents, i.e., canceling noise signals that are common to both channels. [4]

2.1.5 Lock-in Amplifiers

We used three lock-in amplifiers (as shown in the setup above): SR830, SR844 and Ametek for detection of 3 different harmonics and the DC signal.A lock-in amplifier extracts signals with a known carrier wave frequencyand phase from an extremely noisy environment. We used the PEM frequency as the known carrier wave input. In our setup, the SR844 records the second harmonic, the Ametek the first and the third while the SR 830 the DC signal.

2.1.6 Fresnel Rhomb

The double Fresnel rhomb half-wave retarder produces a phase shift of 180° (λ) by the internal

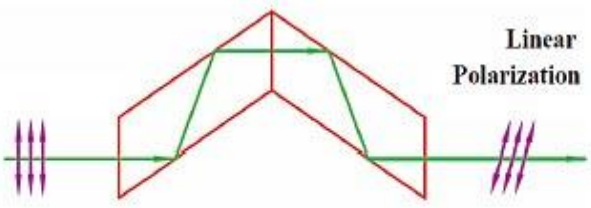

Figure 15: *Tunnel diagram of Fresnel rhomb*

reflections at the four surfaces. This rhomb has input and outputs that are co-axial.[5]

When the incident polarization does not coincide with one of the axes, and the plate is a half-wave plate, then the polarization stays linear, but the polarization direction is rotated. For example, for an angle of 45° to the axes, the polarization direction is rotated by 90° i.e a Θ to 2Θ rotation.[6]

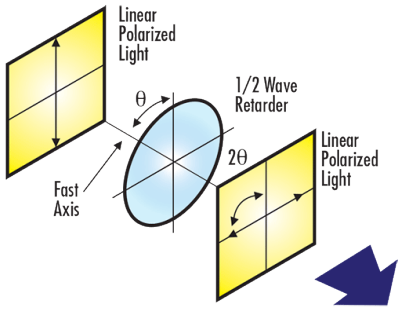

Figure 16: *Half wave plate behaviour*

2.2 Setup Configurations

The experimental setup was used in three different configurations :

5. Single pass
6. Double pass
7. Rotating polarization

2.2.1 Single pass configuration

For this setup the sample was placed on a rotating stage between the source and the NPBS, such that the laser beam only passes through it once as shown in figure 17 below.

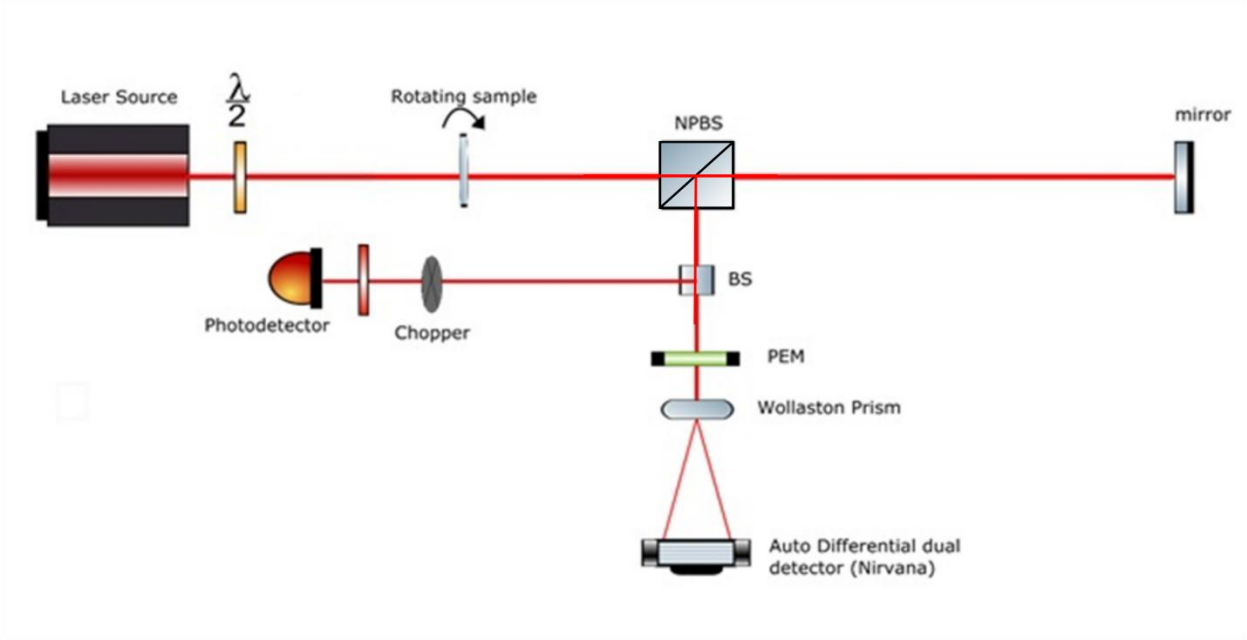

Figure 17: Single pass configuration of MO characterization setup

2.2.2 Double pass configuration

For this setup the sample was placed on a rotating stage between the NPBS and the mirror, such that the laser beam passes through it twice after reflection from the mirror as shown in figure 18 below.

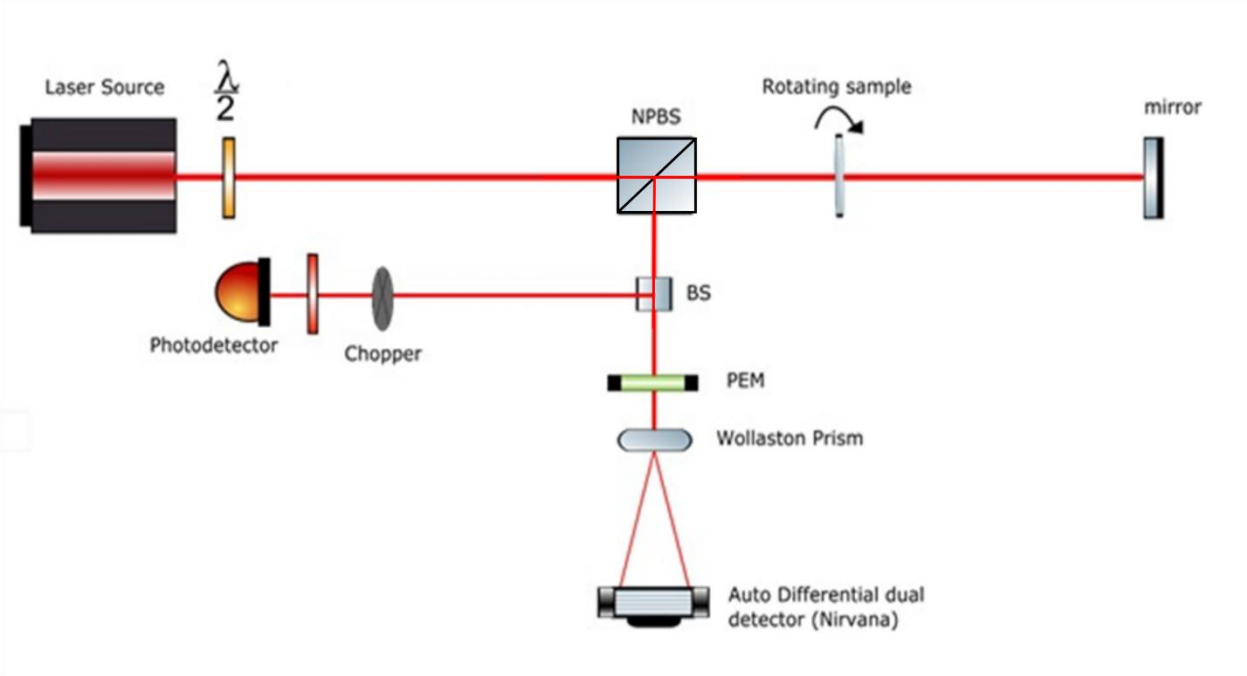

Figure 18: Double pass configuration of MO characterization setup

2.2.3 Rotating polarization configuration

This setup was used to characterize the sample in the presence of a magnetic field by placing the sample in the magnet enclosure such that it is in a double pass scheme with a rotating HWP (Fresnel rhomb prisms used) to rotate the input polarization of the laser beam as shown in figure 19 below.

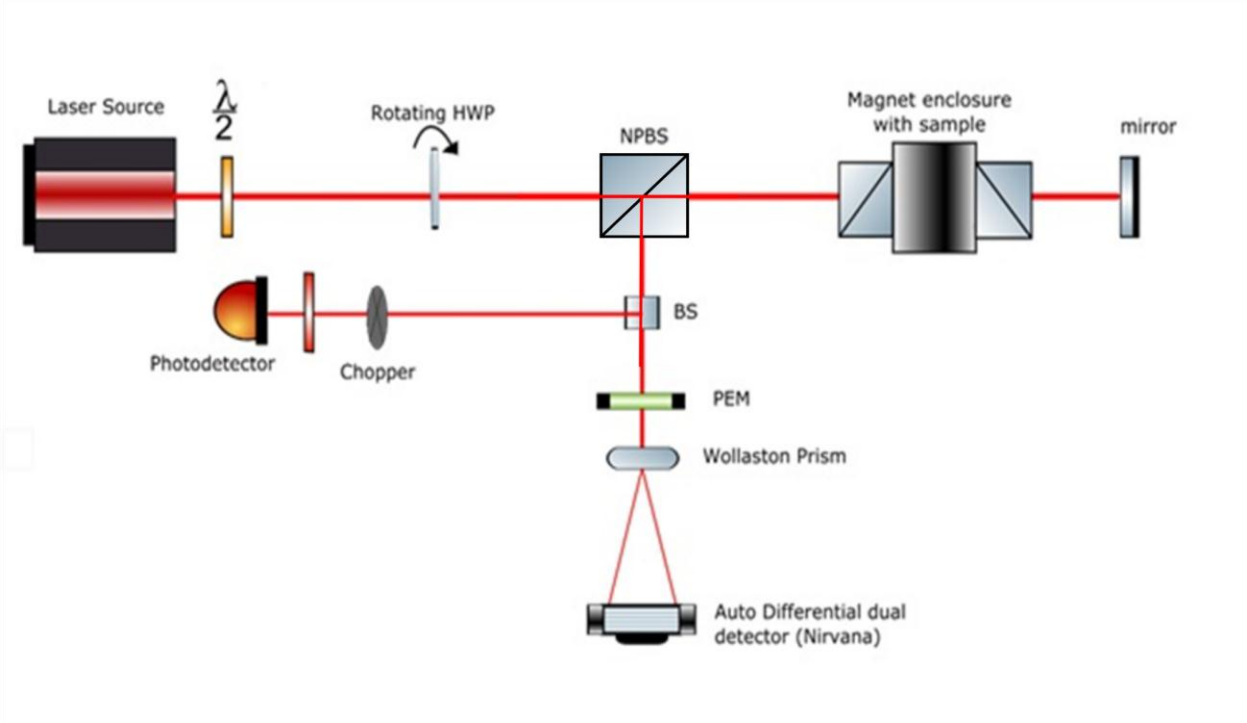

Figure 19: Rotating polarization configuration of MO characterization setup

3. Theory : Mueller Matrix Calculus

The theoretical basis and development required for the determining the Faraday rotation for each of the three experimental configurations described in the previous chapter is based on the Mueller matrix method. Mueller matrices provide the basis for quantitative prediction and for explaining polarization measurements in full detail. Every optical component has a Mueller matrix of four-by-four real valued elements associated with it. The Mueller matrix is an appropriate formalism for characterizing polarization measurements because it contains within its elements all of the polarization properties: diattenuation, retardance, depolarization, and their form, either linear, circular, or elliptical [1]. When the full Mueller matrix for the system is known, then the exiting polarization state is known for an arbitrary incident polarization state .

Normally , these measurements are irradiance measurements (W/m^2) although other flux measurements might be used. The Stokes vector defines the different states of polarizations of the propagating beam. The Stokes vector itself is defined as

$$S = \begin{bmatrix} s_0 \\ s_1 \\ s_2 \\ s_3 \end{bmatrix} = \begin{bmatrix} P_H + P_V \\ P_H - P_V \\ P_{45} - P_{135} \\ P_R - P_L \end{bmatrix} \tag{11}$$

where the variables on the righthandside of (1) correspond to the optical power transmitted through the following:

P_H –a horizontal linear polarizer ,P_V –a vertical linear polarizer, P_{45} –a 45° linear polarizer, P_{135} –a 135° linear polarizer, P_R – a right circular polarizer, P_L – a left circular polarizer

The Mueller matrix **M** for a polarization-altering device is defined as the matrix which transforms an incident Stokes vector **S** into a exiting (reflected , transmitted , or scattered) Stokes vector **S'.**

$$S' = \begin{bmatrix} s_0' \\ s_1' \\ s_2' \\ s_3' \end{bmatrix} = MS = \begin{bmatrix} m_{00} & m_{01} & m_{02} & m_{03} \\ m_{10} & m_{11} & m_{12} & m_{13} \\ m_{20} & m_{21} & m_{22} & m_{23} \\ m_{30} & m_{31} & m_{32} & m_{33} \end{bmatrix} \begin{bmatrix} s_0 \\ s_1 \\ s_2 \\ s_3 \end{bmatrix} \tag{12}$$

The Mueller matrix associated with a system or setup is the multiplication of the Mueller matrices of each polarizing element in the path of the beam. Mueller matrices of some common optical components are listed in Table 1 below.

Table 1: Mueller matrices of common optical components and the corresponding generated Stokes vector [2].

Mueller matrix	**Stokes vector**
Horizontal polarizer $\frac{1}{2}\cdot\begin{bmatrix} 1 & 1 & 0 & 0 \\ 1 & 1 & 0 & 0 \\ 0 & 0 & 0 & 0 \\ 0 & 0 & 0 & 0 \end{bmatrix}$	Horizontally polarized light $\begin{bmatrix} 1 \\ 1 \\ 0 \\ 0 \end{bmatrix}$
Vertical polarizer $\frac{1}{2}\cdot\begin{bmatrix} 1 & -1 & 0 & 0 \\ -1 & 1 & 0 & 0 \\ 0 & 0 & 0 & 0 \\ 0 & 0 & 0 & 0 \end{bmatrix}$	Vertically polarized light $\begin{bmatrix} 1 \\ -1 \\ 0 \\ 0 \end{bmatrix}$
45° linear polarizer $\frac{1}{2}\cdot\begin{bmatrix} 1 & 0 & 1 & 0 \\ 0 & 0 & 0 & 0 \\ 1 & 0 & 1 & 0 \\ 0 & 0 & 0 & 0 \end{bmatrix}$	45° linearly polarized Light $\begin{bmatrix} 1 \\ 0 \\ 1 \\ 0 \end{bmatrix}$

Right circular polarizer $\frac{1}{2}\cdot\begin{bmatrix}1&0&0&1\\0&0&0&0\\0&0&0&0\\1&0&0&1\end{bmatrix}$	Right circularly polarized light $\begin{bmatrix}1\\0\\0\\1\end{bmatrix}$
Left circular polarizer $\frac{1}{2}\cdot\begin{bmatrix}1&0&0&-1\\0&0&0&0\\0&0&0&0\\-1&0&0&1\end{bmatrix}$	Left circularly polarized light $\begin{bmatrix}1\\0\\0\\-1\end{bmatrix}$
Half wave plate at 0° $\cdot\begin{bmatrix}1&0&0&0\\0&1&0&0\\0&0&-1&0\\0&0&0&-1\end{bmatrix}$	
Quarter wave plate at 0° $\cdot\begin{bmatrix}1&0&0&0\\0&1&0&0\\0&0&0&1\\0&0&-1&0\end{bmatrix}$	
Magneto – optic material $M_{sample}=\begin{bmatrix}1&0&0&0\\0&\beta\cos 2\alpha&\beta\sin 2\alpha&0\\0&-\beta\sin 2\alpha&\beta\cos 2\alpha&0\\0&0&0&1\end{bmatrix}$	
Photoelastic modulator $M_{PEM}=\cdot\begin{bmatrix}1&0&0&0\\0&1&0&0\\0&0&\cos\Delta t&-\sin\Delta t\\0&0&\sin\Delta t&\cos\Delta t\end{bmatrix}$	

Using the following matrices from Table 1, Mueller matrix for all the characterization setups in use were calculated.

$$M_{sample} = \begin{bmatrix} 1 & 0 & 0 & 0 \\ 0 & \beta\cos 2\alpha & \beta\sin 2\alpha & 0 \\ 0 & -\beta\sin 2\alpha & \beta\cos 2\alpha & 0 \\ 0 & 0 & 0 & 1 \end{bmatrix} \qquad M_{mirror} = \begin{bmatrix} 1 & 0 & 0 & 0 \\ 0 & 1 & 0 & 0 \\ 0 & 0 & -1 & 0 \\ 0 & 0 & 0 & -1 \end{bmatrix}$$

$$M_{(-45\deg Transmission)} = M_{polariser} = \begin{bmatrix} 1 & 0 & -1 & 0 \\ 0 & 0 & 0 & 0 \\ -1 & 0 & 1 & 0 \\ 0 & 0 & 0 & 0 \end{bmatrix} \qquad M_{PEM} = \cdot \begin{bmatrix} 1 & 0 & 0 & 0 \\ 0 & 1 & 0 & 0 \\ 0 & 0 & \cos\Delta t & -\sin\Delta t \\ 0 & 0 & \sin\Delta t & \cos\Delta t \end{bmatrix}$$

The Mueller matrices are derived for each of the three experimental configurations used in this study:

3.1 Mueller matrix for single pass configuration :

$$I'_{singlepass} = I'_1 = (M_{PEM}) * (M_{mirror}) * (M_{sample}) * (M_{polariser}) * I_1 \tag{13}$$

$$I'_1 = (I_0/2) * \begin{bmatrix} 1 \\ -\beta\sin 2\alpha \\ \beta\cos 2\alpha\cos\Delta t \\ \beta\cos 2\alpha\sin\Delta t \end{bmatrix} \tag{14}$$

Using the following Jacobi Auger expansion in equation for I'_1

$$I'_1 = (I_0/2)[1 - \beta\sin 2\alpha + \beta(\cos 2\alpha)(\cos\Delta t) + \beta(\cos 2\alpha)(\sin\Delta t)] \tag{15}$$

$$\cos(A\cos\omega t) = J_0(A) + 2\sum_{n=1}^{\infty} J_{2n}(A)\cos(2n\omega t)$$
$$\sin(A\cos\omega t) = -2\sum_{n=1}^{\infty}(-1)^n J_{2n-1}(A)\cos(2(n-1)\omega t) \quad (16)$$

where : $\Delta t = A\cos\omega t$

$$I_1^{'} = (I_0/2)[1-\beta\sin 2\alpha + \beta\cos 2\alpha J_0(A) + \beta\cos 2\alpha(J_1(A)\cos\omega t - J_2(A)\cos(2\omega t))] \quad (17)$$

Separating out the AC and DC terms :

$$V_{dc} = (I_0/2)[1-\beta\sin 2\alpha + \beta\cos 2\alpha J_0(A)] \quad (18)$$

$$V_{ac1} = (I_0/2)[2\beta\cos 2\alpha J_1(A)] \quad (19)$$

$$V_{ac2} = (I_0/2)[-2\beta\cos 2\alpha J_2(A)] \quad (20)$$

Defining parameters R_1 and R_2 as follows :

$$R_1 = \left(\frac{V_{ac1}}{V_{dc}}\right) = \frac{2\beta^2 J_1(A)}{1+\beta^2(J_0(A)} \quad (21)$$

$$R_2 = \left(\frac{V_{ac2}}{V_{dc}}\right) = \frac{-2\beta^2 J_2(A)}{1+\beta^2(J_0(A)} \quad (22)$$

$V_{ac\_measured} = 2\sqrt{2}(V_{ac})$ (RMS measured in lock-in amplifier)

choosing A=2.405; $J_0(A)=0$

$$R_1 = \left(\frac{(2\sqrt{2})*(50)*V_{ac1}}{V_{dc}}\right) = \frac{100\sqrt{2}\beta\cos 2\alpha J_1(A)}{1-\beta\sin 2\alpha} \quad (23)$$

$$R_2 = \left(\frac{2\sqrt{2}*(50)*V_{ac2}}{V_{dc}}\right) = \frac{-100\sqrt{2}\beta\cos 2\alpha J_2(A)}{1-\beta\sin 2\alpha} \quad (24)$$

Solving one of the above equations (20) or (21) by squaring both sides and solving for alpha

$$R_1^{\,2} = \left(\frac{100\sqrt{2}\beta \cos 2\alpha J_1(A)}{1-\beta \sin 2\alpha + \beta \cos 2\alpha J_0(A)} \right)^2 \tag{25}$$

$x = 100\sqrt{2}$

$\sin^2 2\alpha(R_1^2\beta^2 + x^2\beta^2 J_1(A)^2) - 2R_1^2\beta \sin 2\alpha + R_1^2 - x^2\beta^2 J_1(A)^2 = 0$

solving quadratic equation in $\sin 2\alpha$

$$\sin 2\alpha = \frac{2R_1^2 \pm xJ_1(A)\sqrt{R_1^{\,2}\beta^2 - R_1^{\,2} + x^2\beta^2 J_1(A)^2}}{2\beta(R_1^2 + x^2 J_1(A)^2)}$$

Solving R_2 gives the same form of eqaution (26)

$$\sin 2\alpha = \frac{2R_2^2 \pm xJ_2(A)\sqrt{R_2^{\,2}\beta^2 - R_2^{\,2} + x^2\beta^2 J_2(A)^2}}{2\beta(R_2^2 + x^2 J_2(A)^2)}$$

3.2 Mueller matrix for double pass configuration :

$$I_{doublepass} = I_2 = (M_{PEM}) * (M_{sample}) * (M_{mirror}) * (M_{sample}) * (M_{polariser}) \tag{27}$$

$$I_2^{'} = (I_0/2) * \begin{bmatrix} 1 \\ 0 \\ \beta^2 \cos^2 2\alpha \cos\Delta t + \beta^2 \sin^2 2\alpha \cos\Delta t \\ \beta^2 \cos^2 2\alpha \sin\Delta t + \beta^2 \sin^2 2\alpha \sin\Delta t \end{bmatrix} \tag{28}$$

$$I_2^{'} = (I_0/2)[1 + \beta^2(\cos^2 2\alpha)(\cos\Delta t) + \beta^2(\sin^2 2\alpha)(\cos\Delta t) + \beta^2(\cos^2 2\alpha)(\sin\Delta t) + \beta^2(\sin^2 2\alpha)(\sin\Delta t)] \tag{29}$$

Using same mechanism of calculation as in single pass :

$$\begin{aligned} I_2^{'} &= (I_0/2)[1 + \beta^2 \cos\Delta t + \beta^2 \sin\Delta t]; \\ &= (I_0/2)[1 + \beta^2(\cos(A\cos\omega t) + \sin(A\cos\omega t))] \\ &= (I_0/2)[1 + \beta^2(J_0(A) + 2\sum_{n=1}^{\infty}(-1)^n J_{2n}(A)\cos(2n\omega t) - 2\sum_{n=1}^{\infty}(-1)^n J_{2n-1}(A)\cos((2n-1)\omega t))] \\ &= (I_0/2)[1 + \beta^2(J_0(A) + 2J_1(A)\cos(\omega t) - 2J_2(A)\cos(4\omega t)] \end{aligned} \tag{30}$$

Again separating out DC and AC terms :

$$V_{dc} == (I_0/2)[1+\beta^2(J_0(A)] \tag{31}$$

$$V_{ac1} = (I_0/2)[2\beta^2 J_1(A)] \tag{32}$$

$$V_{ac2} = -(I_0/2)[2\beta^2 J_2(A)] \tag{33}$$

$$R_1 = \left(\frac{2\sqrt{2}*(50)*V_{ac1}}{V_{dc}}\right) = \frac{200\sqrt{2}\beta^2 J_1(A)}{1+\beta^2(J_0(A))} \tag{34}$$

$$R_2 = \left(\frac{2\sqrt{2}*(50)*V_{ac2}}{V_{dc}}\right) = \frac{-200\sqrt{2}\beta^2 J_2(A)}{1+\beta^2(J_0(A))} \tag{35}$$

A=2.405 and $J_0(A)=0$

$$R_1 = 4\sqrt{2}\beta_1^{\,2} J_1(A) \tag{36}$$

$$R_2 = -4\sqrt{2}\beta_2^{\,2} J_2(A) \tag{37}$$

$$\beta_1 = \sqrt{\frac{R_1}{4\sqrt{2}J_1(A)}}; \tag{38}$$

$$\beta_2 = \sqrt{\frac{-R_2}{4\sqrt{2}J_2(A)}} \tag{39}$$

Hence ,

$\beta = \beta_1 + i\beta_2$ and $|\beta| = \sqrt{\beta_1^{\,2} + \beta_2^2}$

3.3 Mueller matrix for rotating polarization configuration

$$\mathrm{I_B} = (\mathrm{M_{PEM}})*(\mathrm{M_{sample}})*(\mathrm{M_{mirror}})*(\mathrm{M_{sample}})*(\mathrm{M_{HWP}})*(\mathrm{M_{polariser}})*\mathrm{I_0} \tag{40}$$

$$\begin{aligned} I_B^{'} &= (I_0/2)[1-\beta^2\cos\Delta t + \beta^2\sin\Delta t]; \\ &= (I_0/2)[1-\beta^2 J_0(A) - 2\beta^2 J_1(A)\cos(\omega t) + 2\beta^2 J_2(A)\cos(4\omega t)] \end{aligned} \tag{41}$$

$$V_{dc} = (I_0/2)[1-\beta^2(J_0(A)] \tag{42}$$

$$V_{ac1} = (I_0/2)[-2\beta^2 J_1(A)] \tag{43}$$

$$V_{ac2} = (I_0/2)[2\beta^2 J_2(A)] \tag{44}$$

So,

$$\beta_1 = \sqrt{\frac{-R_1}{4\sqrt{2}J_1(A)}}; \tag{45}$$

$$\beta_2 = \sqrt{\frac{R_2}{4\sqrt{2}J_2(A)}} \tag{46}$$

The rotating polarizer setup has an added Mueller matrix of a HWP, which changes the signs of the final equations when compared to the double pass system

4. Results and Discussion

This chapter presents the results of the Faraday rotation experiments and analysis on the the FePt PSP2VP nanocomposite samples.

The results are presented the following order:

(i) Morphology studies
(ii) Anisotropy studies
(iii) Faraday rotation studies

4.1 Morphology studies

Morphology analysis of the samples was done using atomic force microscopy (AFM), magnetic force microscopy (MFM) and friction force microscopy (FFM).

AFM is a type of scanning probe microscopy technique used for force measurements and imaging. It provides the surface topography images of samples as shown in Figure 20 (a) and (b) below. These two pictures show an existence of a certain orientation direction in the deposition of the FePt nanocomposites in the self-assembled block copolymer matrix.

MFM is a derivative of the atomic force microscope. In this technique, a sharp magnetized tip scans the magnetic sample and the tip-sample magnetic interactions are detected and used to reconstruct the magnetic structure of the sample surface as shown in Figure 20(c) .

FFM is also a derivative of the AFM. It optimizes the measurement of the lateral forces that act between a sharp, nanoscopic tip and a surface during scanning of the tip. This technique is used to understand fundamental, molecular scale friction and lubrication processes as seen in Figure 20(d).

All three microscopy techniques show directional linear structures on certain FePt samples, which could be important in further characterization. Hence, this is the basis of our reasoning to conduct further anisotropy studies on these set of samples.

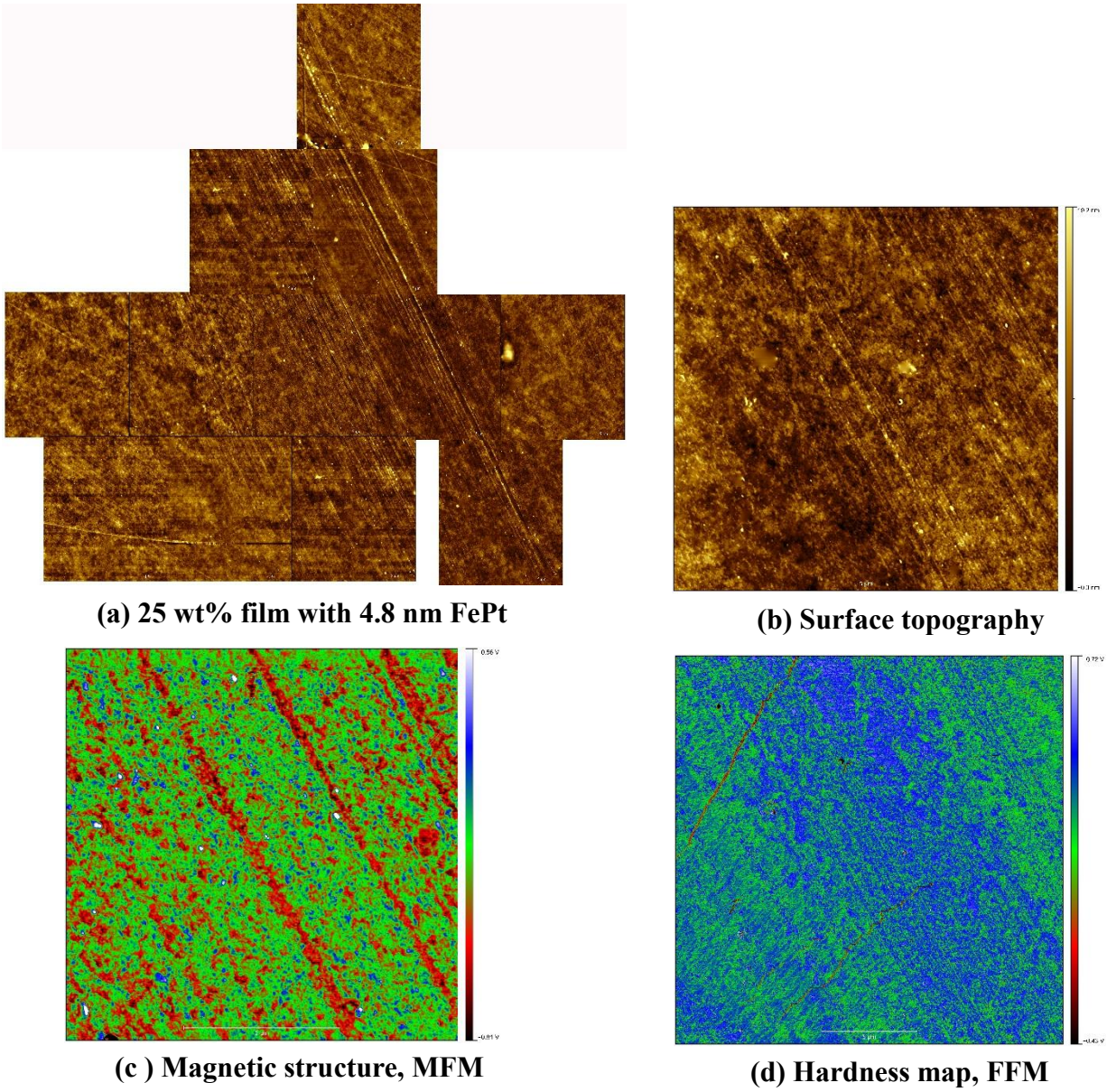

(a) 25 wt% film with 4.8 nm FePt

(b) Surface topography

(c) Magnetic structure, MFM

(d) Hardness map, FFM

Figure 20: Microscopy images of the 25 wt% sample of FePt

To summarize the morphology results :

- all films with 15 – 25wt% 4.8 – 12 nm FePt particles had large scale linear structures on the surface.
- anisotropy factor could be a statistical average.
- orientational ordering was calculated as

$$\gamma = \frac{3}{2}\left\langle cos^2\phi \middle| -\frac{1}{2}\right\rangle$$

with $\phi(\mathrm{r})$ the angle between the vector normal between the block interface and NP ordering.

- linear structures were noticed on most samples which could mean directional dependence of properties.

4.2 Anisotropy studies

Anisotropy studies of the samples were done using the single pass and double pass configurationsas shown in Figures 17 and 18 in Chapter 2. Polar plots of 10 samples of varying wt% of FePt (Figure 21 and 22) were used to identify the minimum depolarization factor β of each sample.

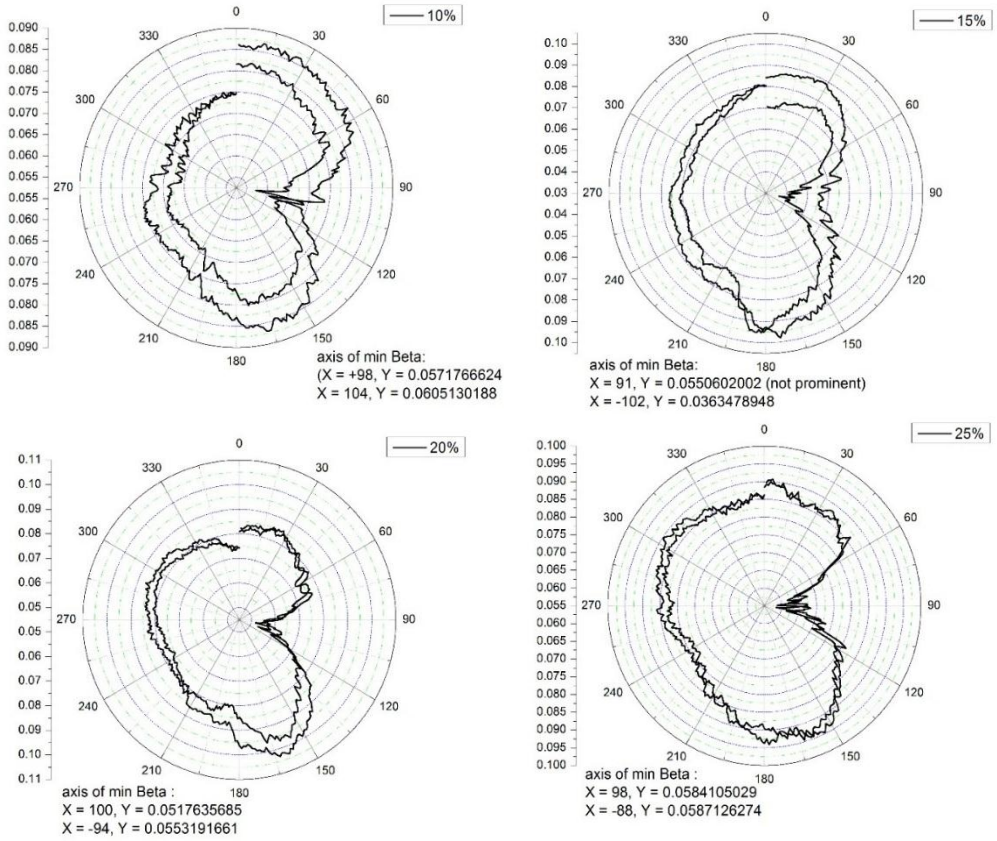

Figure 21: *Polar plots of depolarization factor β analysis for 10%, 15%, 20%, and 25% by wt of FePt nanocopolymer samples*

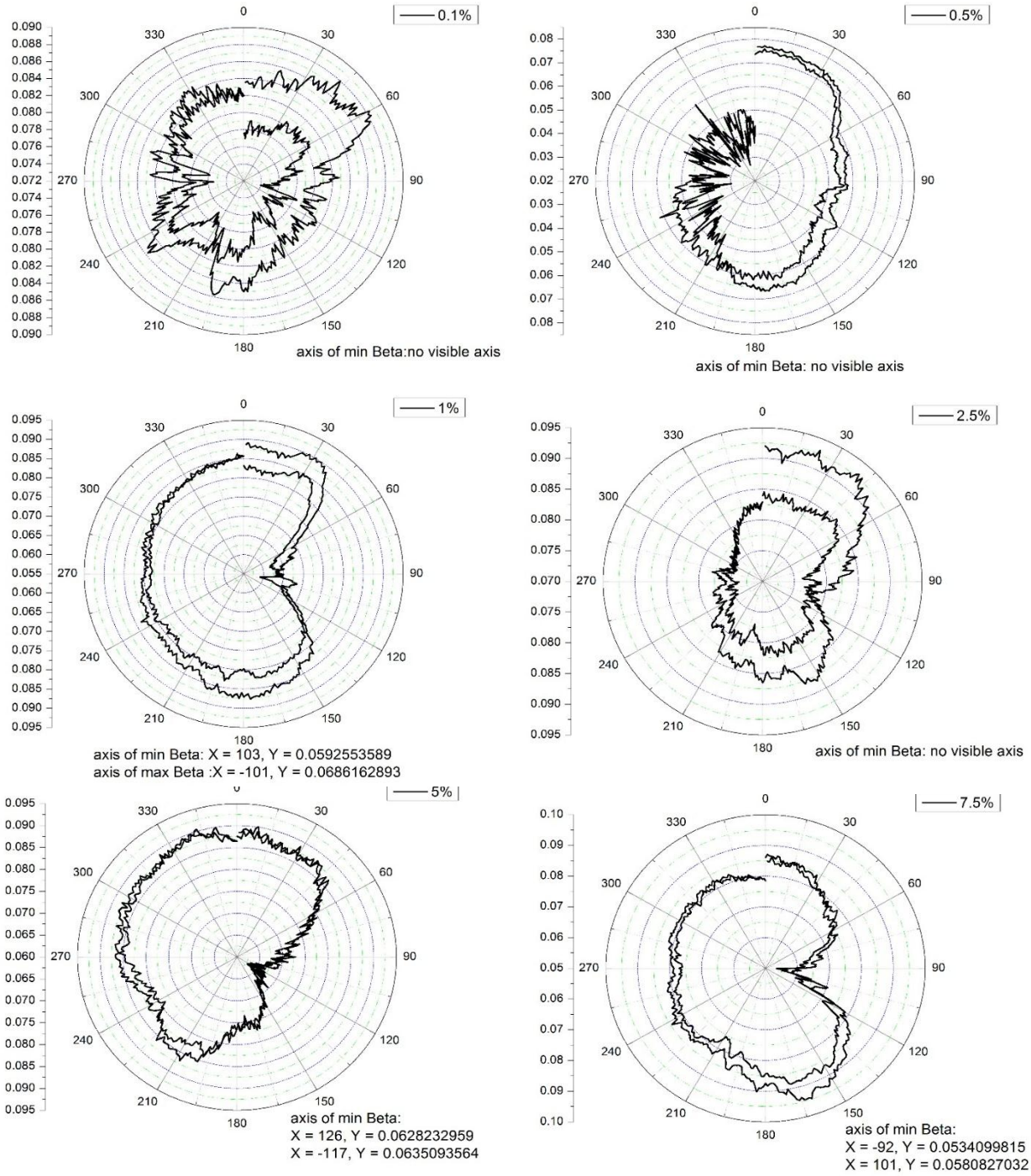

Figure 22: Polar plots of depolarization factor β analysis for 0.1%, 0.5%, 1%, 2.5%, 5% and 7.5% by wt of FePt nanocopolymers

Equation (2) was used to calculate β which was derived using the Mueller matrix approach as explained in Chapter 3. Table 2 shows the values of these depolarization factors with their axis of minimum β values.

Table 1: Minimum Beta values derived using the polar plot

FePtWt % (4.8nm)	**Axis angle**	**Depolarization factor (β)**		
		Positive rotation	**Negative rotation**	**Average**
0.1	-	no axis	no axis	no axis
0.5	-	no axis	no axis	no axis
1	103,-101	0.05926	0.06862	0.06394
2.5	-	no axis	no axis	no axis
5	126,-117	0.06828	0.06351	0.06589
7.5	101,-92	0.05808	0.05341	0.05575
10	98,-104	0.05718	0.06051	0.05885
15	91,-102	0.05506	0.03635	0.0457
20	100,-94	0.05176	0.05532	0.05354

These minimum β values were then plotted against the wt% as shown in Figure 23(b) . Also seen in the figure, the orientational ordering γ of the AFM figures was also plotted against the wt% and show a direct correlation with β.The absorption coefficient data from the Figure 23(a) at 1310nm was used to calculate the MO anisotropy factor which is the ratio of depolarization

factor to the absorption coefficient. This MO anisotropy factor was then plotted against the wt% of FePt as seen in Figure 23(c).

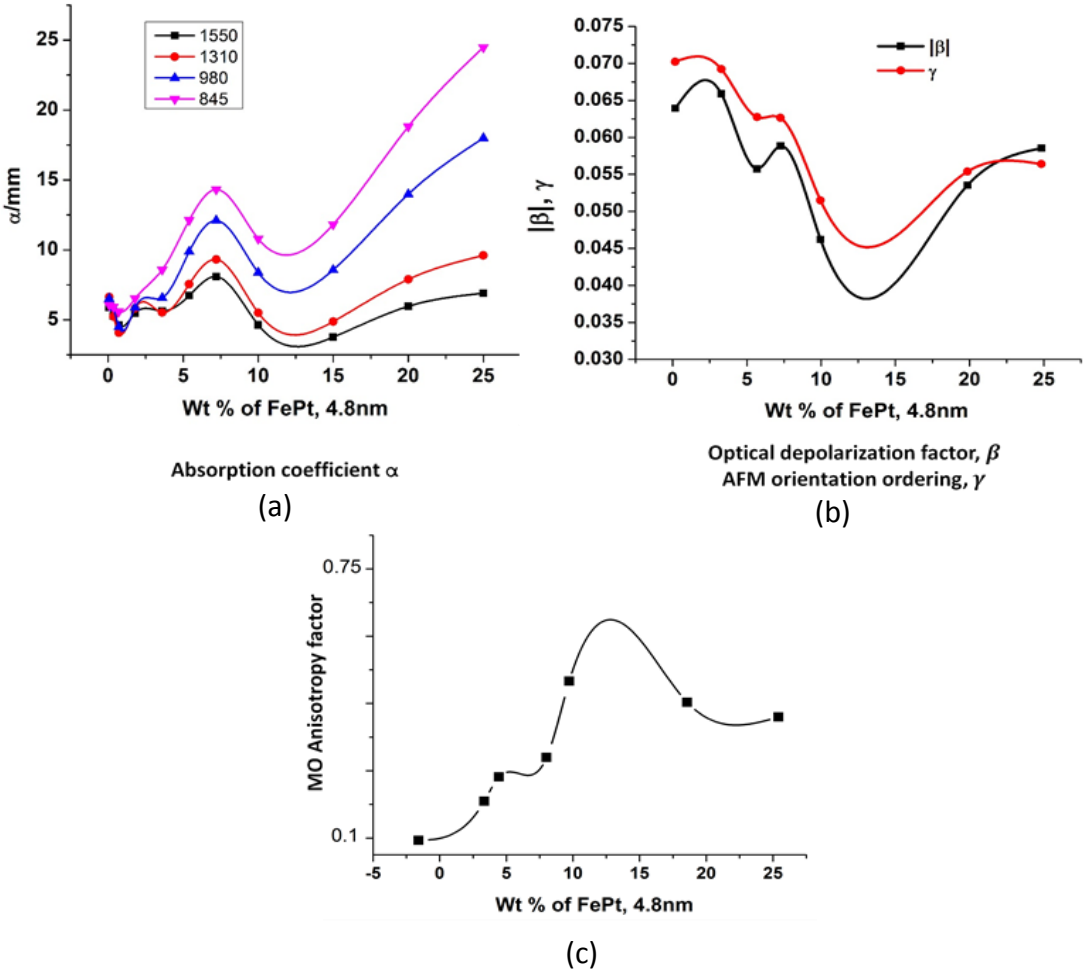

Figure 23: *Graphs representing FePt data plotted against the wt%*

Hence to summarize:

- Some samples had a particular axis of minimum depolarization β while others did not as indicated in Table2. Figure (21 and 22) show the polar plots of these samples.
- There is a correlation between the AFM orientation ordering γ and the presence of a minimum depolarization axis as seen in Figure (23 (c)).
- $MO\ anisotropy\ factor = \frac{\beta}{\alpha}$ shows a general trend of increasing with the increase in wt% of FePt nano particles in the sample.

4.3 Rotating input polarisation in the presence of a magnetic field

The rotating polarization setup was used with an application of + and – 500mT magnetic field. The sample was placed in the sample holder inside the magnetic enclosure as depicted in Figure19 in Chapter 2. The input polarization was rotated using two Fresnel rhomb prisms used as a half waveplate ($\theta \rightarrow 2\theta$).

The depolarization factor in the presence of a magnetic field was calculated using the same Mueller matrix analysis as before. The polar plots in Figure 24 indicate a change in the depolarization factor in the presence of a magnetic field. There are 4 points of minimum beta values. As observed, there is a minimum β value in every quadrant of the polar plot with approximately 90° difference between each minima.

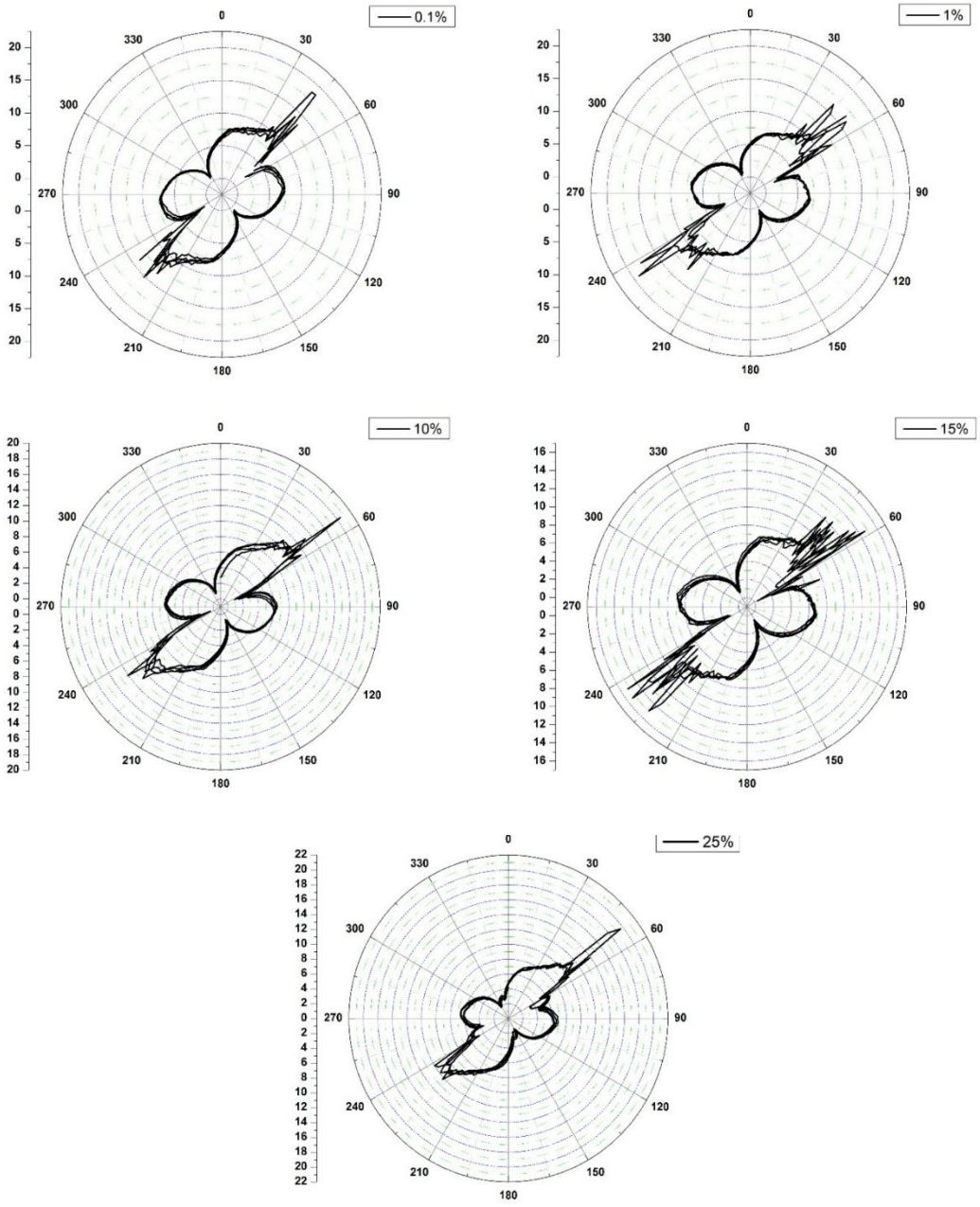

Figure 24: *Polar plots of 0.1%, 1%, 10%, 15% and 25% by wt FePt samples in the presence of a 500mT magnetic field*

Table 2: Depolarization values with and without magnetic field (B)

FePt wt%	Depolarization factor with B field (degrees)	Depolarization factor without B field (degrees)
0.1	1.58494	-
1	1.36013	3.66535
5	-	3.77742
7.5	-	3.19557
10	1.22081	3.37328
15	1.28363	2.62003
20	-	3.06917
25	2.92644	3.35694

The minimum β values were also plotted against the wt% of FePt and the data with magnetic field and without were compared (as seen in Table 3). The β values in the presence of the field were seen to be lower than in the absence of the field, although following a similar trend with the increase in wt% of the FePt nanoparticles as seen in Figure 25.

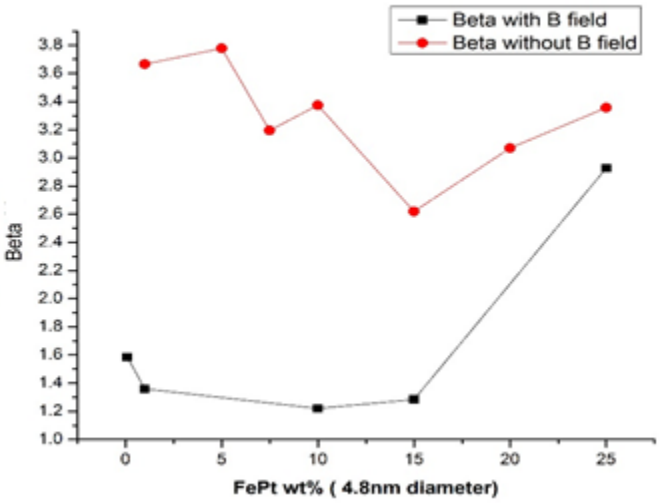

Figure 25: *Comparison of the minimum beta values with and without a magnetic field*

4.4 Conclusion

The following conclusions could be drawn from the experimental observations mentioned above:

- linear structures of the FePt nano particles in the self-assembled block co-polymers could lead to anisotropy in the samples.
- the MO anisotropy factor had a general trend of increasing with the wt% of FePt nanoparticles until approximate 15 wt% , after which it tends to decrease.
- The FePt concentration of 15 wt% is a point of change in MO properties of the samples. More detailed study on the properties around this wt% are required for concrete conclusions to be drawn.

Future scope : A magnetic field sweep to obtain the hysteresis of the samples (from -500mT to +500mT) would help us to understand the magnetic properties to a greater extent.

References

Part I

Spectroscopic Ellipsometry

1. A.A. Khosroabadi, and R. A. Norwood, "Spectroscopic ellipsometry study of novel nanostructured transparent conducting oxide structures," *Photonic and Phononic Properties of Engineered Nanostructures* III, SPIE**8632**, 86320I-1.
2. A.A. Khosroabadi, P. Gangopadhyay,B. Cocilovo, L.Makai, P.Basa,B.Duong, J.Thomas and R.A. Norwood, "Spectroscopic ellipsometry on metal and metal-oxide multilayer hybrid plasmonic nanostructures," OpticsLetters **38**, 3969, doi: 10.1364/OL.38.003969 (2013).
3. R.K. Roy, S.K. Mandal, D. Bhattacharyya, and A.K. Pal1,"An ellipsometric investigation of Ag/SiO2 nanocomposite thin films,"*Eur. Phys. J. B***34**, 25–31, DOI:10.1140/epjb/e2003-00192-5 (2003).
4. F.-Y. Juang, W.-P. Hong, P.R. Berger, P.K. Bhati'acharya, U. Das and J. Singh, "Growth and properties of In052Al0~As/In0~Ga047As,GaAs:In and InGaAs/GaAs multilayers,"*Journal of Crystal Growth* **81**, 377 (1987).
5. https://www.semilab.hu/metrology/ellipsometry/spectroscopic-ellipsometry
6. *Spectroscopic Ellipsometry and Reflectometry: A User's Guide* by H.G.Tomkins, W. A.McGahan
7. https://en.wikipedia.org/wiki/Monochromator
8. http://www.jawoollam.com/tutorial_5.html
9. T.C.Oakberg, "Measurement of waveplate retardation using a photoelastic modulator," SPIE **3121**, 0277-786X/97

Part II :

1. Magneto-optic Characterization

1. Shouheng Sun , "Recent Advances in Chemical Synthesis,Self-Assembly, and Applications of FePt nanoparticles*", Adv Materials*, DOI: 10.1002/adma.200501464

2. M.Stefik, S.Guldin,S. Vignolini, U.Wiesnerd and U.Steiner, "Block copolymer self assembly for nanophotonics," *Chem. Soc. Rev*.**44**, 5076 (2015).
3. K.Aissou, T.Alnasser, G.Pecastaings, G. Goglio, O. Toulemonde, S.Mornet, G. Fleury and G.Hadziioannou, "Hierarchical assembly of magnetic L10-ordered FePt nanoparticles in block copolymer thin films,"*J. Mater. Chem. C***1** , 1317 (2013).
4. B.Rellinghaus, S.Stappert, M.Acet, E. F. Wassermann, "Magnetic properties of FePt nanoparticles," *Journal of Magnetism and Magnetic Materials***266**, 142-154(2003).
5. Michael Bass, Eric W.VanStryland, David R. Williams, William L.Wolfe, *Handbook of Optics*, Volume II (Devices, Measurements and Properties).
6. R. F. Pearson, "Application of magneto-optic effects in magnetic materials,"*Contemporary Physics***14**, 201-211 DOI: 10.1080/00107517308210750 (1973).
7. M.A. Schmidt , L.Wondraczek ,* H. W. Lee , N.Granzow , N.Da,and P. St. J. Russell, "Complex Faraday rotation in microstructured magneto-optical fiber waveguides,"*Advanced Materials***23**, 2681–2688 (2011).
8. http://cddemo.szialab.org/index.html
9. http://www.chem.cmu.edu/groups/Munck/Httpemile/Test7.html#tar115
10. M.Mansuripur, "The Faraday effect,"*Optics and Photonics News* (1999).
11. M.Veis and R.Antos, "Advances in optical and magnetooptical scatterometry of periodically ordered nanostructured arrays," *Journal of Nanomaterials*, vol. 2013, Article ID 621531, 10 pages, 2013. doi:10.1155/2013/621531 (2013).

2. Experimental Setup

1. A.Miles, P.Gangopadhyay, Y.Gai, X.Wang, J.J. Watkins, and R.A.Norwood, "Verdet constant and magnetic permeability in microstructured FePt nanoparticles in PS-P2VP copolymer composite films, SM2G.3, CLEO:2015, OSA 2015
2. P.Gangopadhyay, G.Koeckelberghs, and A.Persoons, "Magneto-optic properties of regioregular polyalkylthiophenes,"*Chem. Mater*.**23**, 516,DOI: 10.1021/cm102215a (2011).
3. http://montanainstruments.com/closed-cycle-optical-cryostat/Magneto-Optic/

4. http://www.hindsinstruments.com/knowledge-center/technology-primer/pem-100photoelastic-modulation/polarization-primer/
5. http://hyperphysics.phy-astr.gsu.edu/hbase/phyopt/cdopt.html
6. Model 2007 & 2017 User's Manual Nirvana Auto-Balanced Photoreceivers (Patent No. 5,134,276)
7. http://www.holmarc.com/fresnel_rhomb_retarders.php
8. https://www.rp-photonics.com/waveplates.html

3. Theory : Mueller Matrices

1. M.Bass, E.W.VanStryland, D.R. Williams, W.L.Wolfe , *Handbook of Optics*, Volume II (Devices, Measurements and Properties)
2. A.Lopez Santiago, *Magneto-optic Polymers and Devices*, 2014 (PhD Thesis)